The effects of support geometry on the turbulence response of loosely supported heat exchanger tubes

M.A. Hassan[1], D.S. Weaver*, M.A. Dokainish

Department of Mechanical Engineering, McMaster University, 1280 Main Street West Hamilton, Ont., Canada L8S 4L7

Abstract

This paper reports the results of numerical simulations of a loosely supported heat exchanger tube excited by turbulence. The effects of support clearance and flow orientation are studied for various support geometries and lattice-bar support offset are investigated. The finite element method was utilized to model the vibrations and the impact dynamics. Three different friction models were examined to account for the tube/support friction forces and issues regarding the efficiency and accuracy of the different techniques are discussed. Tube response and tube/support interaction parameters, such as the impact force, the contact ratio, and most importantly, the integrated product of the contact force and the sliding distance (work rate), are presented. The study indicates that some flow orientations, support types, and support offsets provide favourable support conditions for higher tube sliding motion against the support and, therefore, potentially greater wear rates under service conditions.
© 2003 Elsevier Ltd. All rights reserved.

1. Introduction

Nuclear power plants have experienced problems related to tube failures in steam generators. While many of these failures have been attributed to corrosion, it has been recognized that flow-induced vibrations contribute significantly to tube failure (Païdoussis, 1982). In nuclear steam generators and process plant heat exchangers, tube vibrations are generated by external crossflow. These vibrations may cause severe damage over a relatively short time if vortex shedding resonance or fluidelastic instability occurs. The latter can be especially destructive. In order to avoid these excessive vibrations, tubes are stiffened by placing supports along their length. Various tube/support geometries have been used [see, for example, Weaver and Schneider (1983)], but the majority are either support plates (plates with drilled or broached holes) or flat bars. Unfortunately, clearance is often considered necessary between the tubes and their supports to facilitate tube/support assembly and to allow for thermal expansion of the tubes. As a result, there may be little or no initial contact between some of the tubes and their supports. A combination of flow-induced turbulence and fluidelastic forces may then lead to excessive tube vibration at the supports. While large-amplitude fluidelastic instability can be usually avoided by choosing the location and number of supports properly, the tubes may still vibrate inside their support space due to turbulence excitation. These vibrations cause the tube to impact against and/or slide along the support, which may lead to fretting wear damage and ultimately, tube failure. Such failures may require shut downs resulting in production losses, and pose potential threats to human safety and the environment. Therefore, it is

---

*Corresponding author. Tel.: +1-905-5259140 × 24907; fax: +1-905-572-7944.

E-mail address: weaverds@mcmaster.ca (D.S. Weaver).

[1] Present address: University of New Brunswick, Fredericton, NB, Canada E3B 5A3.

imperative to predict the nonlinear tube response and the associated fretting wear damage to tubes due to fluid excitation.

Gradually, more is being learned about fluid excitation mechanisms. The classification and definition of these mechanisms have been presented in detail by Chen (1978), Païdoussis (1982), and Weaver and Fitzpatrick (1988). Almost all the formulae used in tube-bundle design assume that the tube has a well-defined set of natural frequencies; see for example, Pettigrew and Gorman (1978). This assumption is reasonable when considering tubes with relatively small clearances (Chen et al., 1985). In this case, the tubes are considered to be perfectly supported (support-active). When the clearances are sufficiently large, the tube's support may no longer force a nodal point at its location (support-inactive). The same effect may be produced by corrosion wastage or fretting wear at the tube supports. This makes vibrations and related fluidelastic forces possible in lower modes that have been presumed eliminated by the supports. The resulting tube dynamics are highly nonlinear and very sensitive to support geometry details, tube alignment and clearances [see, for example, Chen et al. (1985)].

A substantial amount of research work has been dedicated to understanding the dynamics of loosely supported tubes. Some of this work was devoted to studying nonlinear tube response while others focussed on characterising tube wear. The work of Chen et al. (1985) focussed on the effectiveness of supports at various excitation levels, while Weaver and Schneider (1983) conducted experiments on U-bend tube configurations with flat-bar supports in the bend region. Their results demonstrated the effectiveness of flat-bar supports in restraining in-plane tube motion. Other experimental studies utilising straight or U-bend tubes have been performed using mechanical excitation (Blevins, 1975; Axisa et al., 1984; Haslinger and Steininger, 1984; Haslinger et al., 1987; Fisher and Ingham, 1989; Connors and Kramer, 1991). Numerical techniques have been developed to compute the response of tubes to fluid excitation. Some of these studies considered tubes with loose baffle plate supports (Rogers and Pick, 1977; Sauvé and Teper, 1987; Rao et al., 1987; Fisher et al., 1989), flat-bar supports (Yetisir and Weaver, 1986; Haslinger and Steininger, 1995; Tan and Rogers, 1996), while others considered broached-hole supports (Fisher et al., 1991).

Axisa et al. (1988) and Fricker (1992) carried out theoretical analyses of loosely supported tubes using various models for fluidelastic instability and reported chaotic-like response. Païdoussis and Li (1992) and Cai and Chen (1993) proved that chaotic oscillations were indeed possible for loosely supported tubes excited by crossflow. The complexity of the dynamics of such systems was further demonstrated in a series of papers by Mureithi et al. (1994a, b, 1995) who showed that the transition to chaos was governed by different mechanisms, depending in part on the type of tube support considered. It is important to note that the transition to chaos is associated with the destabilization of limit cycle oscillations, i.e., it occurs after the tube has become fluidelastically unstable. This research on chaos has important implications for determining the accelerated wear of unstable tubes. However, it is well known that heat exchanger tubes can be rapidly damaged by fluidelastic instability and, therefore, heat exchangers are usually designed to ensure that this does not occur. By keeping the flow velocities below the fluidelastic threshold, turbulence excitation becomes the mechanism of principal concern because it may cause long term wear of the tubes at loose supports. This is the mechanism treated in the present paper.

Most previous research on vibrations of loosely supported tubes has considered flat bars or drilled hole supports. Lattice-bar supports have received relatively little attention in the open literature but are commonly used in heat exchangers such as CANDU nuclear steam generators. Lattice bars substantially increase complexity of tube response because of the influence of flow direction, nonlinear coupling of orthogonal tube modes by these supports and support offset. When using drilled-hole supports, tube dynamics are independent of the flow direction due to the axi-symmetry of the support. However, in the case of lattice-bar supports, flow direction becomes a very important factor affecting the tube dynamics. In addition, lattice-bar supports are usually arranged such that one pair of flat-bars is displaced axially along the tube relative to the other. This is known as support offset and can significantly alter the tube dynamics. In spite of the importance of these factors, their effects have not been covered adequately in the published literature. These issues are addressed in this paper through simulations of the turbulence excited response of tubes in drilled hole, square lattice bar and rhomboid lattice bar supports with various clearances. Several different support friction models are examined. Results are presented and comparisons are made of the effects of all these parameters on contact ratio, impact forces and normal work rate.

The present paper is an extension of the numerical study of Hassan et al. (2002). That paper introduced a set of dimensionless parameters which effectively collapsed the nonlinear response of turbulence excited tubes in loose rhomboid lattice bar supports. The flow direction was fixed parallel to an axis of symmetry of the supports and only a single support offset was considered. For the sake of clarity and completeness, the theoretical model and dimensionless parameters developed in that paper are briefly reviewed below.

2. Tube/support model

2.1. Impact modelling

The mathematical modelling of the tube/support impact used herein was described in detail and verified in Hassan et al. (2002). Briefly, the impact of the tube against the support is modelled by a spring of stiffness (K_{imp}) added at the support location when the normal component of the tube displacement (u_n) exceeds the radial support clearance (C_r). In addition, the hysteresis damping of impact is modelled and no significant permanent indentation is assumed. The contact force (F_{imp}) is then modelled as a function of the relative tube/support overlap which is given by

$$F_{imp} = K_{imp}(|u_n| - C_r) + C_{imp}\dot{u}_n, \tag{1}$$

where the $\dot{u}_n$ is the normal component of the tube velocity. An expression for the damping coefficient (C_{imp}) is obtained by equating the kinetic energy lost by the impacting body to the energy dissipated in the system due to impact (Hunt and Crossley, 1975).

$$C_{imp} = K_{imp}\beta(|u_n| - C_r), \tag{2}$$

where β is a damping parameter that depends on the coefficient of restitution of the impacting bodies. The value of the support damping coefficient (β) used in this work was 0.25 s/m for steel (Hunt and Crossley, 1975).

To calculate the time history of the tube response, a pseudo-force algorithm was used. In this procedure, impact forces were assumed to be known and the corresponding response was computed using the standard finite element solution of the beam equation:

$$[M]\{\ddot{u}\} + [C]\{\dot{u}\} + [K]\{u\} = \{F_e(t)\} + \{F_{imp}(u, \dot{u}, t)\}, \tag{3}$$

where F_e represents the external forces (turbulence, fluidelastic, etc.) which are assumed known. Tube response is obtained by integrating Eq. (3) while disregarding the tube/support contact. Based on the tube response obtained, clearance, and type of support impact forces are then calculated. The process is repeated until convergence is attained in the impact forces. The entire problem is projected onto the unsupported tube eigenmodes. This permits solving for the system response while saving considerable computational effort. The aforementioned model was implemented in INDAP, an in-house finite element code (Dokainish, 1988) and was verified against several documented examples (Hassan et al., 2002).

2.2. Fluid excitation modelling

The tube was assumed to be fluidelastically stable and, therefore, turbulence forces are the only source of excitation. In general, fluid excitation due to turbulence is modelled as randomly distributed forces. The bounding power spectral density (PSD) measured by Oengören and Ziada (1995) was utilised in this research. Depending on the flow velocity and the tube's diameter, the PSD curve of the turbulence excitation is obtained. Finally, this PSD curve is transformed into a force–time record using an inverse Fourier transform algorithm. Two different force-versus-time records were used to represent the fluid excitation in the lift and the drag directions. The lift force record contains only a fluctuating force component with a zero mean. On the other hand, the drag force record consists of a fluctuating force component superimposed on a static component representing the steady drag forces. These are then input into the nonlinear tube/support model. These forces were assumed to be fully correlated along the span of the tube. However, the two force components, drag and lift, are fully uncorrelated.

2.3. Friction Modelling

Friction forces arise when the tube moves tangentially relative to the support surface. While friction between the tube and the support can dissipate energy, it causes damage as well. Therefore, modelling friction at the tube/support interface is important. However, no generally accepted mathematical model has yet been developed to accurately describe this phenomenon. Coulomb friction is usually applied to contact problems because of its simplicity. However, sliding-direction velocity chatter occurs when using the Coulomb friction model due to the sharp discontinuity in the friction force near the zero-sliding velocity. Karnopp (1985) developed a friction model in which a zero velocity interval, $\{-V_0, +V_0\}$ defines the sticking friction regime. Within this zone, the friction force is determined such that it balances the net forces applied to the system. Haessig and Friedland (1991) developed a "bristle model" to capture the microscopical contact points between the two surfaces. The point of contact is thought of as a bond between flexible bristles. When one surface moves relative to the other, bristles, which are formed randomly on the surface, act as

springs representing the sticking friction force. As the relative displacement of a bristle exceeds a certain value, the bond snaps and a new one is formed at another location. The accuracy of the model depends on the number of bristles. However, the model is numerically inefficient due to its complexity.

The "velocity limited friction model" (VLFM) was employed previously in loosely supported tube simulations (Rogers and Pick, 1977; Fisher et al., 1991; Yetisir and Weaver, 1986). In this model, a limiting velocity (V_0) is used to overcome the difficulties associated with the discontinuity of the classical Coulomb friction model. Depending on the value of the sliding velocity (V_t), the friction force is either an arbitrary function of the velocity (a linear function is used in the above studies) or equal to the dynamic friction capacity, F_f:

$$F_f = -\text{sign}(V_t)\mu_d F_N \quad \text{if } V_t > 0,$$
$$F_f = -\text{sign}\left(\frac{V_t}{V_0}\right)\mu_s F_N \quad \text{if } |V_t| \leqslant V_0,$$

(4)

where μ_d and μ_s are the coefficients of dynamic and static friction, respectively, and F_N is the normal force. Antunes et al. (1990) developed a "spring-damper friction model" (SDFM), in which the sticking force is obtained by introducing an adherence stiffness and an adherence damper:

$$F_f = -\text{sign}(V_t)\mu_d F_N, \qquad \text{sliding,}$$
$$F_f = -\text{sign}(V_t)(K_a(u_c - u_0) + C_a V_t), \quad \text{adherence,}$$

(5)

where K_a and C_a are the adherent stiffness and damping, respectively, and u_c and u_0 are the current and zero-velocity tangential displacements, respectively. Using this model, they presented simulations of a loosely supported tube with varying preloads. Their results showed that large preloads substantially reduce the normal work rate as one would expect since there is less sliding contact. Tan and Rogers (1996) extended the Karnopp model to simulate friction in multi-degree of freedom systems and heat exchanger tubes. They designated their model as the "force-balance friction model" (FBFM). The sticking is tested when the absolute velocity is less than a small limiting velocity (V_0). Friction force during sticking is calculated such that it balances the net force:

$$F_f = ku - F_e,$$

(6)

where ku represents the internal forces at the point of contact. In order for sticking to occur, this force must satisfy the inequality $F_f < \mu_s F_N$, otherwise sliding occurs. Simulation results for the SDFM, VLFM and FBFM friction models are compared in Section 3.3.

3. Simulation results

3.1. Dimensionless parameters

The dimensionless parameters developed by Hassan et al. (2002) are reviewed briefly and will be used to present the current results. The radial tube/support clearance, C_r, is normalised by the r.m.s. resultant tube response with its support inactive, d_{rsi}, i.e., the tube response at the support location obtained by applying the same excitation on the linear unconstrained system. Thus, the dimensionless clearance is C_r/d_{rsi}. The r.m.s. impact force, F_{imp}, is normalised by the total r.m.s. turbulence force, i.e., the product of the distributed turbulence force per unit length, F_{tur}, and the tube length, L. Thus, the dimensionless force is $F_{\text{imp}}/(F_{\text{tur}}L)$. The fluid excitation is expressed in terms of the reduced flow velocity, $U_R = U/fd$, where U is the mean flow velocity normal to the tube, f is the tube's natural frequency and d is the tube's diameter. Normal work rate, W_N, is normalised by the input power induced by turbulence, W_{tur}. The total power absorbed by a tube of length, L, and mass per unit length, m, was expressed by Yetisir et al. (1997):

$$W_{\text{tur}} = \sum_{i=1}^{n} \frac{S_{FF}(f_i)J_i^2 L}{2m},$$

(7)

where $S_{FF}(f_i)$ and J_i^2 are the PSD of the local force per unit length in the ith mode and the joint acceptance, respectively. Thus, the dimensionless normal work rate is W_N/W_{tur}. The lift, d_y, and drag, d_z, displacements of a point at a distance, x, from the fixed end are normalised by the r.m.s. lift, d_{ysi}, and drag, d_{zsi}, response of the unconstrained configuration (tube with support inactive), respectively.

3.2. Tube/support modelling

A cantilever tube of 617 mm length, 15.88 mm outer diameter, and 0.8 mm wall thickness was utilised in these simulations. The equivalent mass per unit length and elasticity modulus are 0.32 kg/m and 106 GPa, respectively. Simulations were carried out using 24 flexural modes each having 1% damping. The tube was loosely supported at the free end as shown in Fig. 1. A support stiffness of 10^5–10^7 N/m has been reported in the literature (Rogers and Pick, 1977; Axisa et al., 1988) and a value of 10^6 N/m was used in the present study. However, these papers demonstrated that the impact forces are rather insensitive to the support stiffness in this range. The support damping factor, β, used in this work was 0.25 N s/m. A single coefficient of friction value of 0.1 was utilized since this value represents a reasonable lower bound. For each case study, five seconds of response time history were computed. The tube/support interaction parameters were averaged over the simulation time record, excluding the initial transient period of about 0.5 s.

Three types of supports are studied in the present paper: drilled-hole (DH), square flat-bar (SFB), and rhomboid flat-bar (RFB) supports, as shown in Fig. 2. As mentioned earlier, the drilled-hole support is obtained by drilling an oversized hole in a plate (Fig. 2(a)) and was utilised in some of the early steam generator designs. Drilled-hole supports are structurally strong and provide excellent tube support. However, the annular support area around each tube is not well vented for the release of steam and impurities. As well, drilled-hole supports may severely block the flow, especially as corrosion deposits develop (Weaver and Schneider, 1983). Due to the geometry of the DH support, the tube-to-support clearance is the same in all directions, provided that the tube is centred. The SFB support (Fig. 2(b)) consists of two pairs of flat bars (pairs A and B) perpendicular to each other. The tube-to-support clearance in the drag and lift directions is equal to the nominal radial clearance. The nominal radial clearance for a centred tube is the clearance between the tube and its supports in the direction perpendicular to one of the support pairs. In comparison, the RFB support (Fig. 2(c)) consists of two pairs of flat bars, which form a diamond-shaped support space. In the case of the RFB support (Fig. 2(c)), the ratio of the clearance in the drag and lift directions to the nominal clearance are 2 and 1.155, respectively, for the case in which the flow direction is parallel to the support axis ($\varphi = 0$). In the case of a DH support, the tube/support contact occurs at a single point. However, with SFB and RFB supports, tube/support contact may occur either at a single point on one support bar or at two points when the contact occurs with the tube in one of the corners between two flat bars.

3.3. Effect of friction modelling

Simulations were conducted to investigate the three different friction models (VLFM, SDFM, and FBFM) discussed in Section 2.3. Numerical simulations were carried out to address two aspects: comparative prediction performance and numerical efficiency. It is not possible to evaluate accuracy because of the paucity of reliable experimental data regarding tube/support friction. Simulation results using the three models are shown in Fig. 3. The effect of the steady drag force component is studied by varying the drag coefficient in the range of 0.1–1.0. The effect of the steady drag force on the contact ratio is shown in Fig. 3(a). Increasing the drag coefficient increases the steady force component which in turn increases the normal force preload of the tube against the support. Thus, as one would expect, increasing the steady drag force increases the ratio of the contact time to total time (contact ratio) from zero to a value approaching unity, i.e., from no contact to nearly continuous contact. Increasing steady the drag force also increases the r.m.s. impact force (Fig. 3(b)). A reference turbulence excitation force (resultant excitation force with a drag coefficient of 1.0) was used here to normalize the impact force. Fig. 3(c) shows the effect of the drag coefficient on the mid-span lift response. Dimensionless lift response decreases gradually as the drag force increases until a minimum value is reached at a drag coefficient of 0.6.

As can be seen in Figs. 3(a)–(c) the friction model used in the analysis has very little effect on the contact ratio, impact force, and tube lift response. However, friction modelling does have an effect on the normal work rate estimate (Fig. 3(d)). The effect is negligible up to a drag coefficient of about 0.6, above which the stick-slip models, SDFM and FBFM, predict lower normal work rates than the VLFM. This is attributed to the fact that at high steady drag force values, the friction force increases, and the sticking effect becomes significant. The largest difference in the normal work rate of the VLFM prediction, compared to the SDFM and the FBFM predictions, was found to be about 9.1% and 8.8%, respectively, and this occurred at the largest drag coefficient used (1.0). A detailed comparison of the results is shown in Table 1.

Fig. 4 illustrates the effect of the friction coefficient on the tube response predictions for a dimensionless clearance of 0.21 and a drag coefficient of 0.60. Increasing the coefficient of friction results in a slight increase in the contact ratio (Fig. 4(a)) and a slight decrease in the dimensionless r.m.s. impact force (Fig. 4(b)) and dimensionless tube mid-span lift response (Fig. 4(c)). The choice of friction model has a negligible effect on these parameters. On the other hand, as the coefficient of friction is increased, the dimensionless work rate is significantly decreased. This is attributed to the
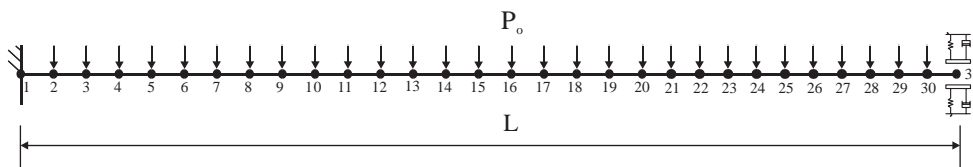
Fig. 1. Tube/support model.
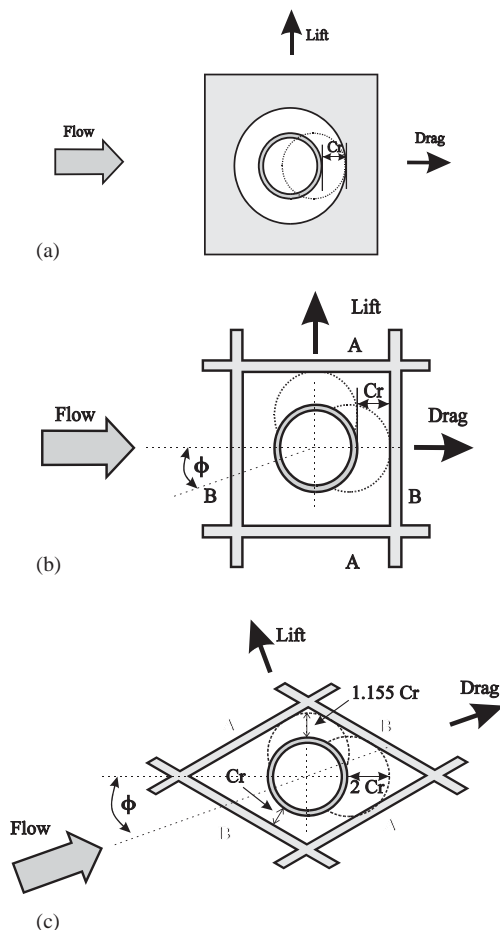
Fig. 2. Types of tube supports: (a) Drilled-hole support (DH); (b) Square-flat bar support (SFB); and (c) Rhomboid-flat bar support (RFB).

increase in the friction capacity which limits the tangential (sliding) motion. The same behaviour is obtained using the three friction models. It can be seen that the dimensionless work rate prediction of the SDFM and FBFM are consistently slightly lower than the VLFM counterpart. As the coefficient of friction increases, the deviation in the normal work rate prediction of the VLFM compared with the SDFM and FBFM predictions increases, the maximum difference being about 8.0% at a coefficient of friction of 0.5. predictions increases, the maximum difference being about 8.0% at a coefficient of friction of 0.5.

Numerical efficiency is assessed by considering the computer processing time. A time step of 10 μs was found to provide numerical stability when using the VLFM for all the drag coefficient values. For both the SDFM and the FBFM, a time step of 10 μs was adequate for a stable simulation considering drag coefficients up to 0.6. Beyond a drag coefficient of 0.6, the SDFM and the FBFM models require a smaller time step to ensure numerical stability and hence a larger simulation time. In addition, the choice of time step for the FBFM was found to be less restrictive than that for
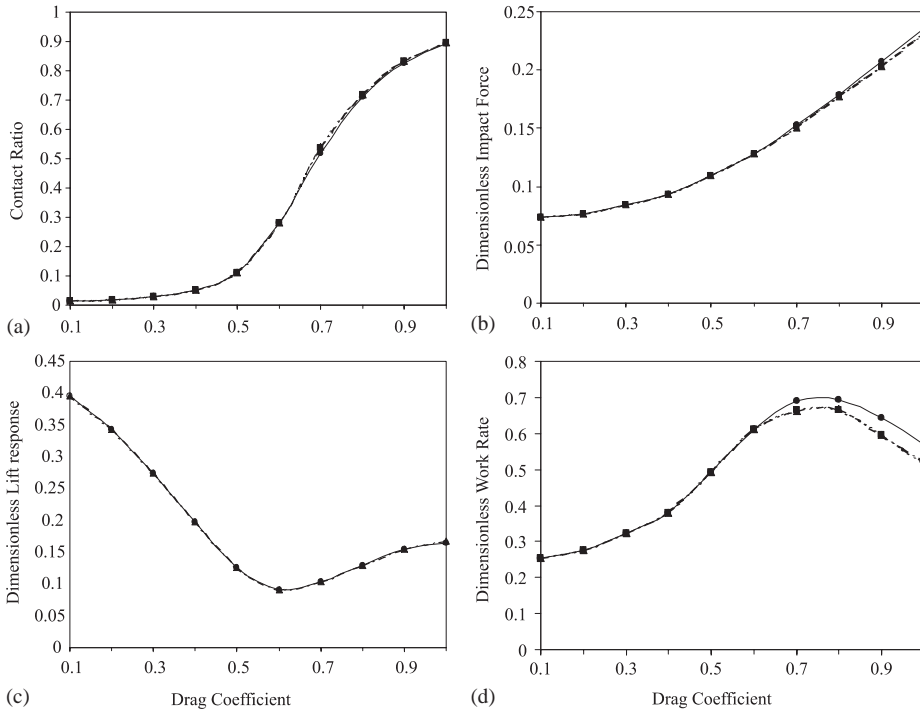
Fig. 3. Dimensionless tube response vs. drag coefficient utilizing different friction models for a dimensionless clearance of 0.20 and friction coefficient of 0.1: ●, VLFM; ▲, SDFM; ■, FBFM: (a) Contact ratio; (b) r.m.s. impact force; (c) r.m.s. lift response; (d) normal work rate.
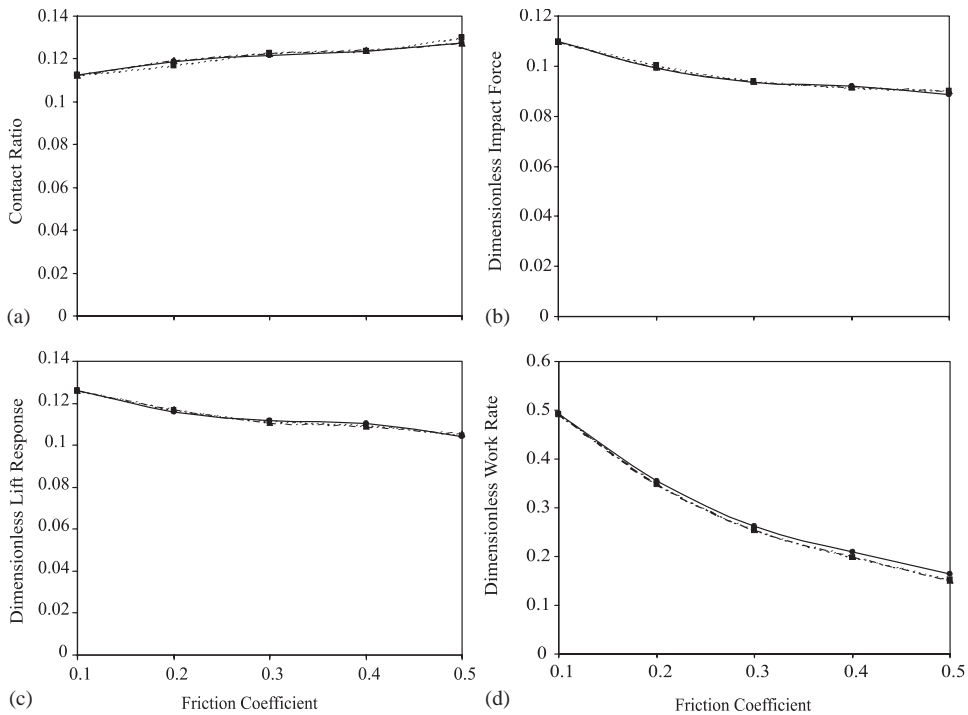
Fig. 4. Dimensionless tube response vs. friction coefficient utilizing different friction models for a dimensionless clearance of 0.20 and a drag coefficient of 0.6: ●, VLFM; ▲, SDFM; ■, FBFM: (a) Contact ratio; (b) r.m.s. impact force; (c) r.m.s. lift response; and (d) normal work rate.

Table 1
Comparison of typical tube response calculations using three different friction models for the case dimensionless clearance of 0.21, drag coefficient of 1.0, and friction coefficient of 0.1

	VLFM	SDFM (using model of Antunes et al., 1990)	FBFM (using model of Tan and Rogers, 1996)
Dimensionless impact force	0.2361	0.2319	0.2313
Contact ratio	0.8908	0.898	0.8979
Dimensionless mid-span lift response	0.1646	0.1669	0.1669
Dimensionless normal work rate	0.5667	0.5149	0.5191
Time step (μs)	10	1	5
Simulation time (min)	212.5	568	430.5

the SDFM. However, it requires more simulation time than that of the VLFM. Using the SDFM and the FBFM, extra simulation times of 167% and 103%, respectively, were required to ensure numerical stability as compared with the VLFM.

In the present research, the tube is assumed to be centred in its supports with a small preload. The VLFM was utilized since it provides reasonable accuracy with substantial savings in computation times (see Table 1). Sticking, which tends to prevent wear, is not well addressed in this model. However, because the preloads and friction coefficient used here are relatively small, the error in using the VLFM will be small and conservative (overestimate the normal work rate). The SDFM or the FBFM would be required if an initial contact or a significant preload were considered.

3.4. Effect of support geometry

3.4.1. General response characteristics

Since the use of dimensionless parameters collapses the results at different excitation levels (flow velocities) over a single curve (Hassan et al., 2002), a single reduced flow velocity, $U_R = 13.5$, is used in the present analysis. The linear response of a single-span tube is generally dominated by the response of the fundamental mode. Since clearance at the support leads to support impact, higher modes may participate significantly in tube vibration. Fig. 5 shows samples of the lift response PSD of a tube with a RFB support. This tube is subjected to a flow parallel to the support axis ($\varphi = 0$ in Fig. 2). The spectra presented are for tubes subjected to the same reduced flow velocity (13.5) but with different dimensionless clearances. Depending on the clearance value, two groups of frequency peaks can be easily identified. For a small clearance (Fig. 5(a)), the PSD of the tube response is dominated by frequencies corresponding to the natural frequencies of the fixed-hinged configuration (support-active). At large clearances, the PSD of the tube response is dominated by the lower frequency free modes of the tube (support-inactive), as shown in Fig. 5(d). Figs. 5(b) and (c) depict the PSD of the tube response for intermediate clearances in which a transition between the modes takes place. This behaviour is known as the mode switch. Note that the response spectra appear noisy with rather poorly defined natural frequencies. Similar response spectra are also observed in the drag direction.

Fig. 6 shows the lift response spectra of an SFB supported tube. The lift response spectrum for a dimensionless clearance of 0.01, Fig. 6(a), shows the presence of a cluster of low-frequency peaks around 17 Hz, in addition to a strong peak at 110 Hz (the first constrained mode). Increasing the dimensionless clearance further to 0.35 causes the 110 Hz peak to disappear while other peaks appear at frequencies around those of the unconstrained system, Fig. 6(b). The frequencies of these peaks continue to gradually approach those of the unconstrained modes, Fig. 6(c). Eventually, at a large dimensionless clearance, the frequencies coincide with the frequencies of the unconstrained system. The tube's motion in the drag direction is constrained by support pair B due to the drag force, while the lift motion is resisted only by the friction forces. This causes an early mode switch in the tube lift response. These results are in marked contrast to those of the RFB support as seen in Fig. 5. The latter behaviour is due to the fact that the mean drag forces cause the tube to become wedged into the corner of RFB supports for the flow direction considered here, thereby substantially restraining the lift response when clearance is small.

Fig. 7 shows samples of the lift response PSD of a tube with a DH support with four different clearances. Similar to the RFB support, two groups of frequency peaks can be easily identified depending on the clearance value. For a small clearance, Fig. 7(a), the PSD of the tube response is dominated by frequencies corresponding to the natural frequencies of the fixed-hinged configuration (support-active). At large clearances, the PSD of the tube response is dominated by the lower frequency free modes of the tubes (support-inactive) as shown in Fig. 7(d). In the case of the RFB support, the transition between the support-active and the support-inactive regimes occurs suddenly around a dimensionless
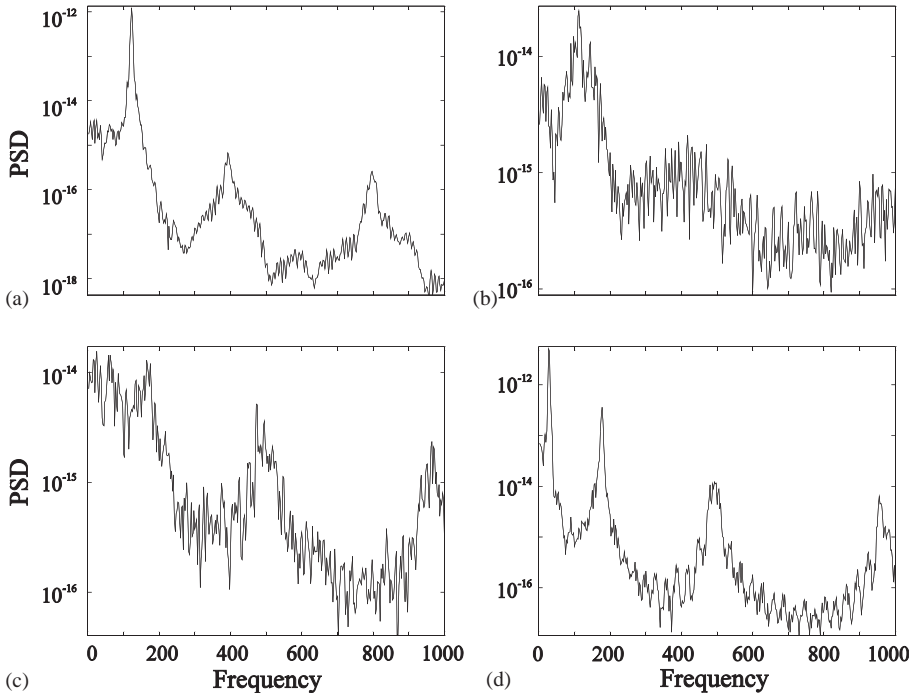
Fig. 5. Lift response spectra for various dimensionless clearances (RFB support): (a) 0.01; (b) 0.4; (c) 0.45; and (d) 0.8.
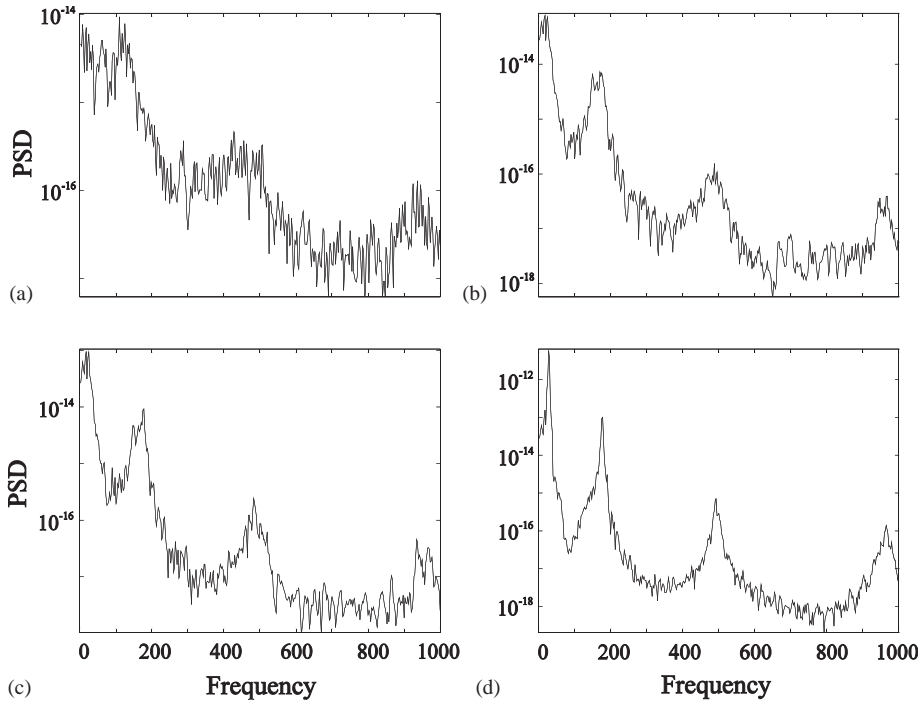
Fig. 6. Lift response spectra for various dimensionless clearances (SFB support): (a) 0.01; (b) 0.35; (c) 0.45; and (d) 1.0.

clearance of 0.4. However, the transition from the support-active to the support-inactive modes in the case of the DH support proceeds gradually over the entire range of support clearances studied here (0–1.3). As indicated in Figs. 7(b) and (c), the frequency of the fundamental mode decreases gradually starting from 122 Hz (the fundamental mode of the
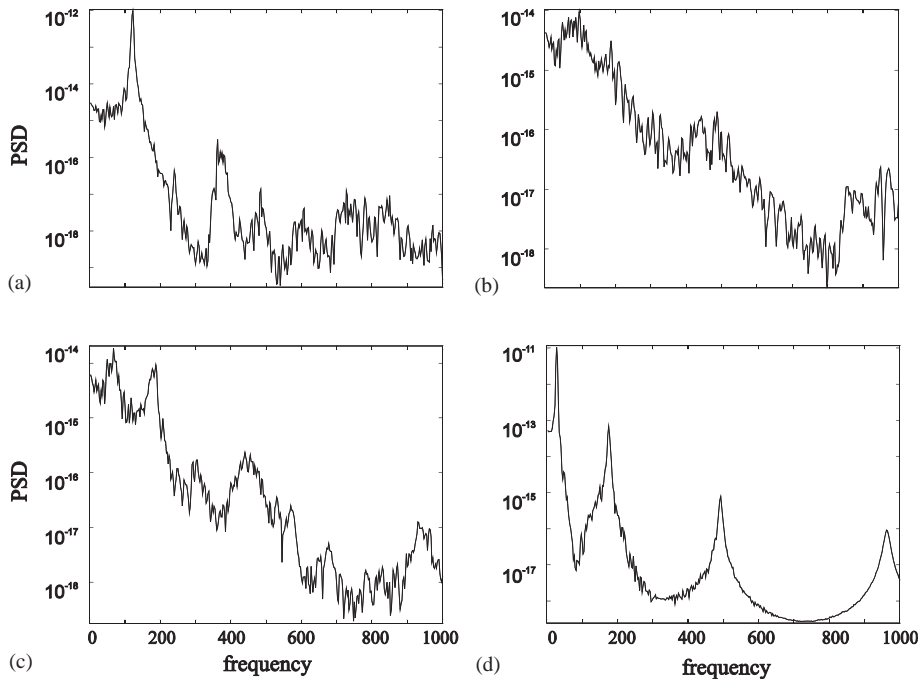
Fig. 7. Lift response spectra for various dimensionless clearances (DH support): (a) 0.001; (b) 0.05; (c) 0.1; and (d) 1.3.
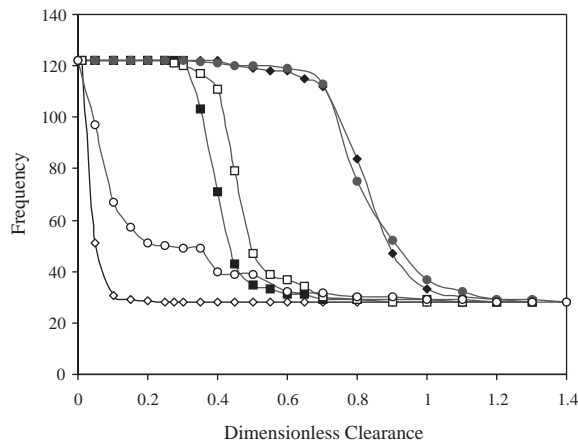
Fig. 8. The fundamental frequency of the tube for various support cases; open symbols (lift direction), closed symbols (drag direction): ○,●, DH; ◇,◆, SFB; ■,□, RFB.

constrained system) to 28 Hz (the fundamental mode of the unconstrained system), while the second natural frequency gradually decreases from a value of 398–176 Hz.

Fig. 8 compares the variation in the fundamental frequency of the lift and drag response for the three support arrangements. The fundamental frequency of the drag response remains constant at a value of 122 Hz, the frequency of the support-active mode, for a range of dimensionless clearances. A sharp drop in the frequency marks the transition from the support-active to the support-inactive modes. This behaviour is maintained for all support arrangements. For SFB and DH supports, the drag direction mode switch occurs at a dimensionless clearance of about 0.8. This is because in the drag direction both the SFB and DH supports have the same effective clearance which is equal to the nominal clearance in these cases. As mentioned above, the effective clearance in the drag direction is twice the nominal clearance

in the case of the RFB support. As a result, the mode switch occurs at a dimensionless clearance which is approximately one-half that of the DH and SFB supports.

In the case of the RFB support, the clearance available in the lift direction is linearly dependent on the tube's position within the support space. If the tube is in the centre of the support space, the clearance in the lift direction is at its maximum value (115% of the nominal clearance). On the other hand, if the tube is in the support corner, the clearance available in the lift direction is zero. Hence, the tube's motion in the drag direction affects the tube's vibrations in the lift direction. In the presence of the steady drag forces, the tube's centre is shifted to the support corner where the tube's lift motion is effectively constrained by support pairs A and B. This situation may also exist due to tube misalignment. In other words, the effective support clearance is largely reduced in this situation. The lift response frequency of the RFB support is slightly higher than that of the drag response for a narrow range of dimensionless clearances (0.4–0.6) as seen in Fig. 8.

In the case of a SFB support, the tube's vibration in the lift direction is opposed by both pair A and the friction forces generated at pair B. In addition, the instantaneous clearance available in the lift direction is constant and equal to the nominal support clearance. Since the lift excitation is less than that of the drag direction, the tube has more contact with pair B than pair A. As the clearance increases, the tube's lift response is not large enough to cause tube/support contact with pair A. As a result, the lift direction mode switch in the case of the SFB support occurs at a relatively low support clearance. On the other hand, the drag direction mode switch does not occur until the clearance is relatively large, 0.8.

Similar to the RFB support, the clearance available in the lift direction for a tube in a DH support varies with the tube's position. However, this clearance varies quadratically with the tube's drag displacement. The transition from support-active to support-inactive modes in the lift direction occurs at rather low clearances, similar to but more gradually than that of the SFB support. In the drag direction, the transition takes place at a higher clearance, essentially the same as that for the SFB support.

The above discussion shows how sensitive the frequency response and mode switch are to support geometry, nominal clearance and mean flow direction. This is further illustrated in Fig. 9 which gives the tube's centre trajectories for a particular case of nominal clearance and flow velocity. Note that the drag force pushes the tube into the corner of the RFB support, Fig. 9(a), thereby limiting the tube's motion. On the other hand, more sliding occurs for the SFB and DH supports as shown in Figs. 9(b) and (c), respectively. Thus, at least for the flow direction considered, SFB and DH supported tubes are expected to have similar response characteristics and produce greater wear rates.
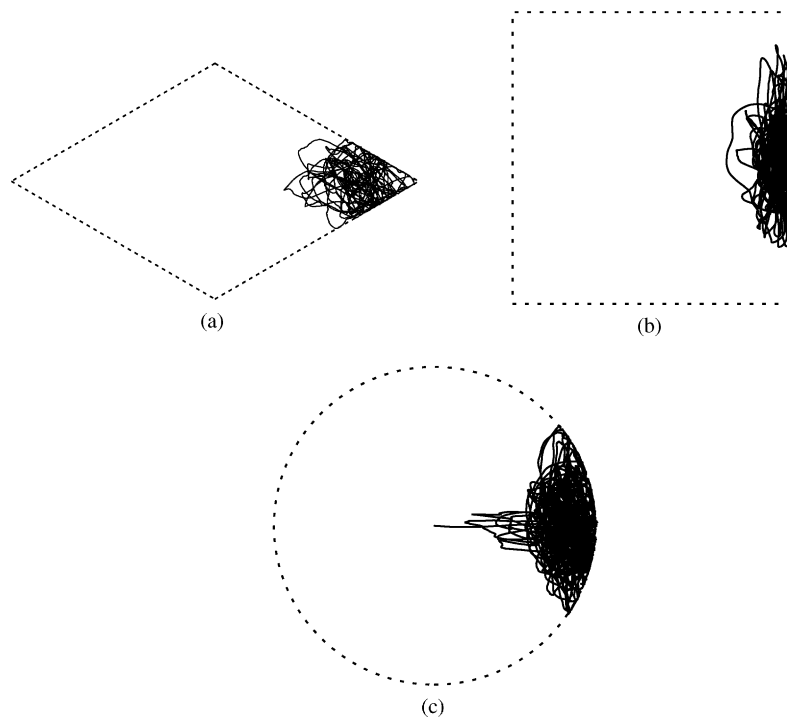
Fig. 9. Tube tip trajectory for various support types: (a) RFB; (b)SFB; and (c) DH.

3.4.2. Geometry effect on contact, response, and work rate

To determine the general features and differences amongst the various types of supports, details of the tube/support interaction at each of the support pairs are presented. The two pairs in the RFB support are at equal angles (30°) to the flow direction. Therefore, the tube has an equal probability of contact with either pair regardless of any differences in the force applied in the lift and drag directions. In the case of the SFB support, each of these pairs is perpendicular to one of the excitation directions (drag or lift). Hence, contact with either pair depends on the excitation level in the lift and the drag directions. Fig. 10(a) depicts the contact ratio of a DH support as well as that of both pairs for the SFB and RFB support configurations as a function of support clearance. The contact ratio is defined as the summation of the time intervals during which the tube/support contact is maintained, divided by the total duration of the time record. The total duration of the time record selected is sufficiently large that the results are independent of the length of the time record. The contact ratio for pairs A and B are identical in the case of the RFB support as expected. The RFB support exhibits a higher contact ratio than that of the SFB support for pair A (the lift direction support) which drops dramatically to zero at a dimensionless clearance of 0.1 because contact no longer occurs with these supports. On the other hand, the contact ratio for pair B of the SFB supports decreases to zero at a much higher dimensionless clearance ($C_r/d_{rsi} > 1.2$). As expected from the discussion in the previous section, the contact ratio for DH supports is very similar to that for support pair B of the SFB supports. The drop in the contact ratio caused by the mode switch from support-active to support-inactive modes occurs at approximately twice the dimensionless clearance as for RFB supports. This is due to the fact that the effective drag direction clearance in the latter case is double the nominal clearance for the other cases.

A similar behaviour is expected for the r.m.s. impact force since it is dependent on the contact ratio. The RFB support exhibits an identical r.m.s. impact force level for both pairs as shown in Fig. 10(b). On the other hand, the SFB support exhibits a higher impact force level at pair B (drag direction) than at pair A (lift direction). The impact force level in the case of the DH support is similar to that of pair B of the SFB support.
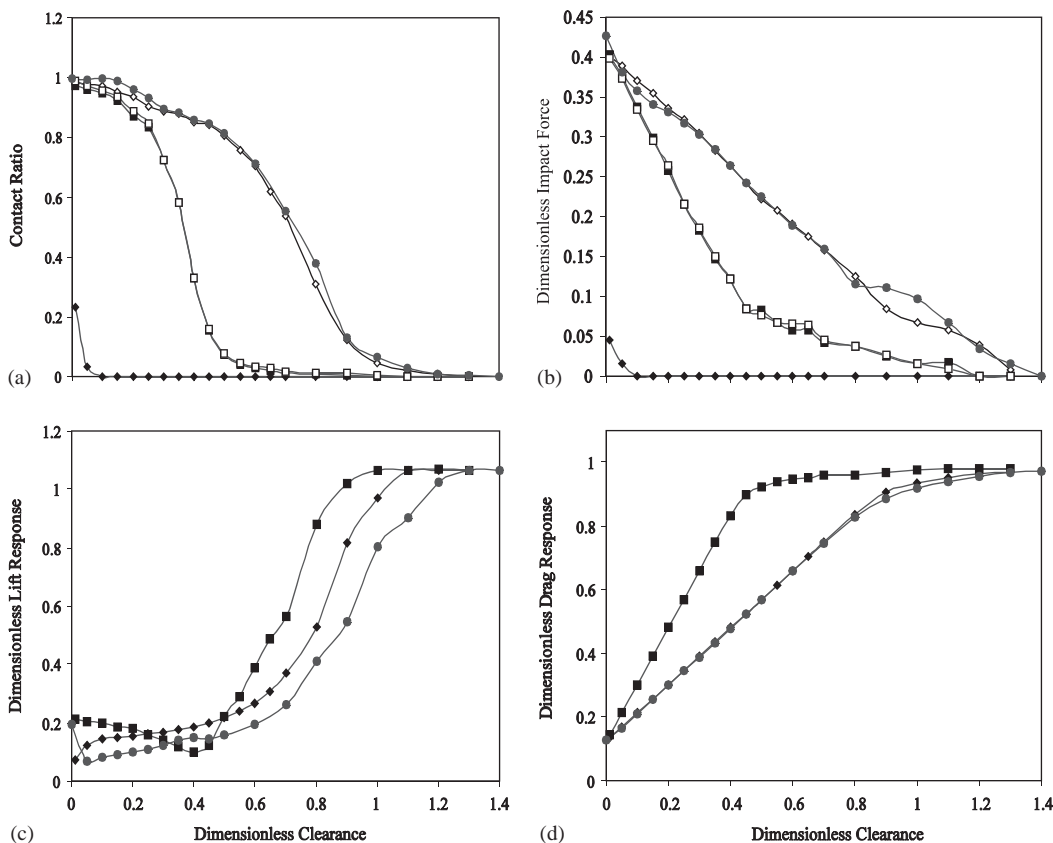
Fig. 10. Dimensionless tube response vs. dimensionless clearance for various support cases: open symbols (pair B), closed symbols (pair A): ○,●, DH; ◇,◆, SFB; ■,□, RFB: (a) contact ratio; (b) r.m.s. impact force; (c) r.m.s. lift response; and (d) r.m.s. drag response.

The r.m.s. tube response in the lift direction for the three support geometries is shown in Fig. 10(c). The RFB support exhibits a characteristic behaviour. Up to a dimensionless clearance of about 0.05, the tube response decreases gradually. The support then becomes inactive, leading to the mode switch. These results in the evolution of low-frequency modes and a further increase in the clearance will yield an increase in the tube response. The latter will finally approach the response level of the linear unconstrained system at a dimensionless clearance of about 1.0.

In the case of the SFB support, three different response regions can be identified. Initially, the tube's lift response increases rapidly in the dimensionless clearance range 0.0–0.1 due to an early mode switch in the lift direction. In the second region, $0.1 < C_r/d_{rsi} < 0.6$, the tube's response increases at a relatively low rate. In this clearance range, only friction forces resist the tube's motion in the lift direction because there is no contact between the tube and the support pair in the lift direction. The normal forces at the support caused by steady drag forces on the tube control the effect of these friction forces. In the third region, less contact is maintained, which leads to a lower friction resistance at the tube/support interface. This is manifested by a greater increase in the response rate beyond a dimensionless clearance of 0.6 until it approaches asymptotically the support inactive condition near a dimensionless clearance of 1.1.

In the case of the DH support, the lift response drops rapidly to minimum at a dimensionless clearance of 0.05, which corresponds to the dimensionless clearance at which the mode switch begins. As the clearance increases, the tube's lift response gradually increases. This is attributed to a gradual decrease in the tube's natural frequency as indicated by the response spectra for this support.

Dimensionless drag response is depicted in Fig. 10(d). As mentioned earlier, the ratio of the effective clearance to the nominal clearance for the SFB and RFB supports in the drag direction are 1 and 2, respectively. Therefore, the displacement in the drag direction (for the range of clearance/excitation values that provides a support-active end condition) for the RFB support is twice that of the SFB and the DH supports. If the effective drag direction clearance was used in Fig. 10(d) rather than the nominal clearance, the curves for the three different support cases would essentially collapse to a single curve.

The predicted normal work rates at each support pair for the SFB and RFB supports are presented in Fig. 11(a). The work rate at pairs A and B for the RFB supports are identical. However, the work rate for pair A of the SFB supports is much higher than that for the RFB supports. These results are not surprising since the geometry of the SFB support promotes more sliding motion and therefore, a higher work rate. For the flow direction being considered, the impact force in the case of the RFB support always has a component in both the lift and the drag directions. This imposes resistance to the sliding motion of the tube along the flat bars in an RFB support. However, friction against pair B is the only resistance to the tube's motion in the lift direction (perpendicular to pair A) if no contact is maintained with pair A of the SFB supports. This has a significant effect on the total work rate, which is higher in the case of the SFB supports as shown in Fig. 11(b). This figure shows that the SFB and DH supports exhibit much higher work rates than the RFB supports for all clearances greater than 0.05. The total work rate (summation of work rates obtained from pairs A and B) of the DH support is lower than that of the SFB support for a dimensionless clearance in the range of 0.15–0.8. In the case of the DH support, the total work rate shows two peaks at dimensionless clearances of 0.1 and 0.8 which represent the mode switch points for the lift and drag directions, respectively. For dimensionless clearances larger than 0.8, the total work rate of the DH case is essentially the same as that of the SFB case.

3.5. Effect of flow orientation

The flow field in heat exchangers or steam generators is characterised by a mean velocity which varies in direction relative to the tube bundle geometric pattern depending on the location within the unit. Such flow distributions are typically determined by thermohydraulic analysis. To determine the effects of the flow direction relative to support geometry, numerical simulations are presented for the single-span tube considered above. Flow angles ranging from $0°$ to $180°$ are investigated with an average of 21 radial clearance values per flow angle. These simulations were carried out considering a tube supported by a loose RFB support, as shown in Figs. 1 and 2(c). Clearly, flow orientation will have no effect on DH supports and the flow orientation considered above will be a worst case for the SFB supports.

The contact between the tube and a specific support pair is dependent on the flow direction. When the flow angle is zero, the flow direction is at an angle of $30°$ with either pair as seen in Fig. 2(c). Therefore, the contact ratio for both pairs is the same. As the flow direction changes, the tube maintains an unequal contact ratio with both pairs. The contact ratio is expected to be higher at the pair with the larger angle with regard to the drag direction. Fig. 12(a) depicts the contact ratio between the tube and support pair A for various flow orientations. For a given relatively small support clearance, the contact ratio decreases gradually as the flow angle increases. It then decreases sharply to a minimum at a flow angle of $60°$, at which the flow is in the direction of the minimum clearance between the tube and support pair B, i.e normal to pair B. Increasing the flow angle beyond $60°$ results in an increase in the contact ratio for pair A. For a given flow angle, increasing the radial clearance decreases the contact ratio as the mode switch occurs. For
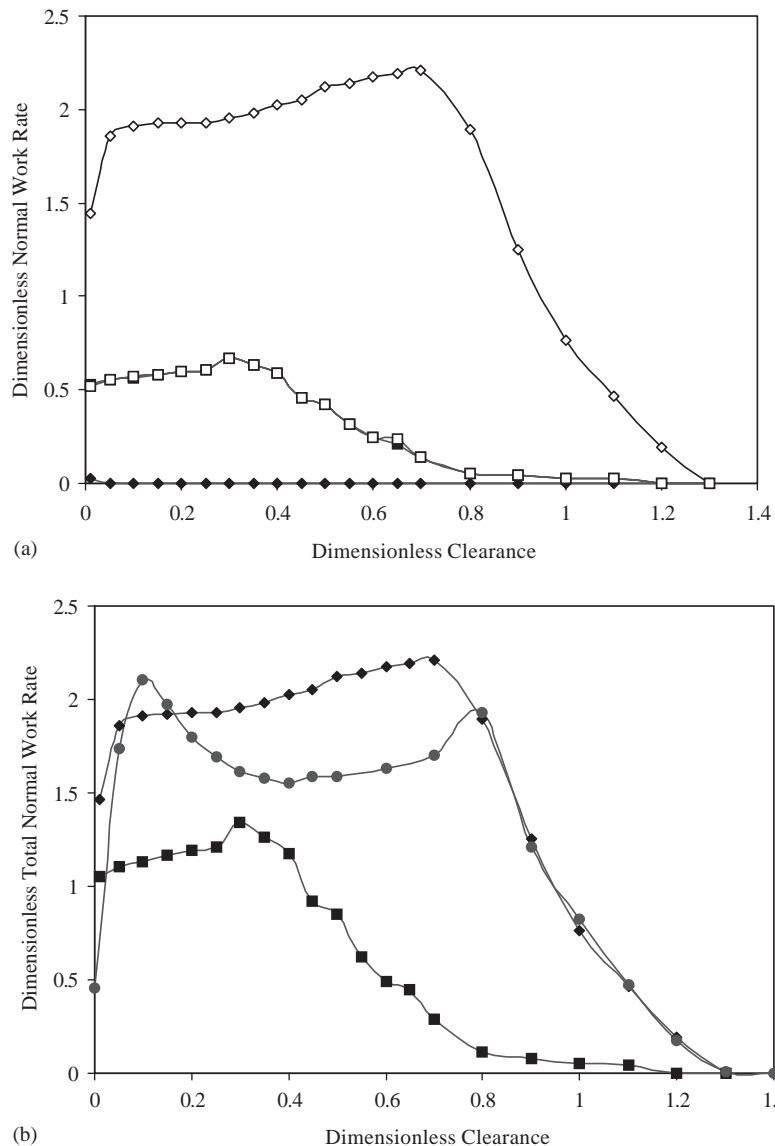
Fig. 11. Dimensionless normal work rate for various support cases; open symbols (pair B), closed symbols (pair A): ○, ●, DH; ◇, ◆, SFB; ■, □, RFB: (a) each support pair and (b) total.

small clearances, flow angles in the range of 100–180° appear to have little effect on the contact ratio for pair A. However, as the clearance increases, flow angles in the range of 100–180° cause the contact ratio to decrease gradually. This is followed by a sharp drop accompanying the mode switch.

The r.m.s impact forces resulting from the tube impacting with pair A are shown in Fig. 12(b). The general behaviour of the dimensionless impact force follows that observed for the contact ratio. At an angle of 60°, the flow is normal to pair B and, therefore, the impact forces on pair A are at a minimum. The dimensionless impact force then increases gradually to a maximum at a flow angle around 150° where the flow is parallel to support pair B.

The predicted normal work rates at support pair A are presented in Fig. 12(c) in dimensionless form. For a given flow orientation, the general trend of the work rate with increasing clearance is similar. The normal work rate increases gradually as the clearance increases. The increase in the work rate continues to a certain clearance where less contact is being maintained and the mode switch occurs. The mode switch marks the transition of the tube dynamics from the fixed-pinned to the fixed-free end condition. At this point, less contact occurs and the work rate drops. For a given support clearance, the dimensionless work rate for support pair A decreases gradually as the flow angle increases. The
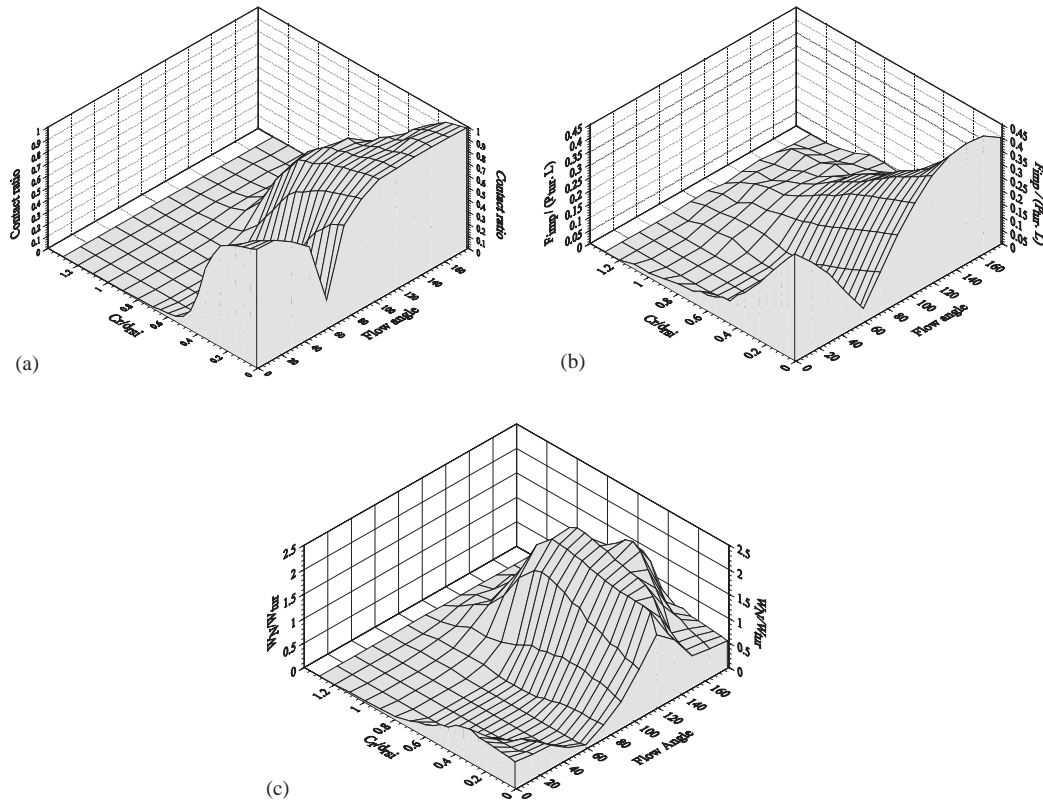
Fig. 12. Dimensionless tube response vs. dimensionless clearance for various flow orientations for support pair A: (a) Contact ratio; (b) r.m.s. impact force; and (c) work rate.

minimum work rate is obtained at a flow angle of 60° which is normal to pair B. Thus, friction at pair B is the most significant resistance to tube motion and the work rate is expected to be at a maximum for the flow orientation for pair B and at a minimum for pair A. This is demonstrated by the maximum wear rate for pair A occurring at a flow orientation of 120° in Fig. 12(c). At this flow angle, the flow is normal to pair A. For small clearances, the contact ratio is high and the r.m.s. impact forces significant as seen in Figs. 12(a) and (b). Therefore, the normal work rate is at a maximum for pair A and will be at a minimum for pair B. Indeed, the results for contact ratio, r.m.s. impact force and normal work rate for pair B will be identical to those for pair A but shifted by 60°, which is the angle between the support pairs. It is noteworthy that at a flow orientation of around 120°, the flow is normal to support pair A, the effective clearance in the drag direction is at a minimum, and the mode switch (drop in contact ratio) is delayed to a higher dimensionless clearance as seen in Fig. 12(a). Thus, the normal work rate at the flow orientation actually increases with increasing clearance to a dimensionless clearance of 0.7.

The tube response in the presence of loose supports presents a large variety of contact conditions. These range from continuous contact, to contact with occasional lift-offs, to intermittent occasional contacts. These contact conditions were investigated by examining the trajectories of the tube response at the support. Fig. 13 shows a sample of the tube displacement trajectories at a flow angle of 15° for various dimensionless clearances. For a small clearance, Fig. 13(a), the tube's drag forces push the tube against the support corner. For a slightly higher dimensionless clearance, Fig. 13(b), more sliding motion is permitted. Tube lift-off is continuously resisted by the drag, while sliding as well as motion in the lift direction, are resisted by both pairs. Moreover, the tube maintains approximately equal contact with both pairs. For a larger dimensionless clearance, Fig. 13(c), the tube maintains more contact with pair B than with pair A. Hence, the tube motion exhibits a higher sliding behaviour along pair B. A further increase in the support clearance causes the tube to impact and slide against pair B only (Fig. 13(d)). Thus, the wear on support A would be reduced to zero and would be higher for support B.

The response (lift) spectra of a tube subjected to crossflow at a 30° flow angle are shown in Fig. 14. The tube's response depicts the domination of its constrained modes at a small clearance as shown in Fig. 14(a). As the clearance increases, the higher frequency peaks become flattened out as contact becomes more intermittent. At a clearance of
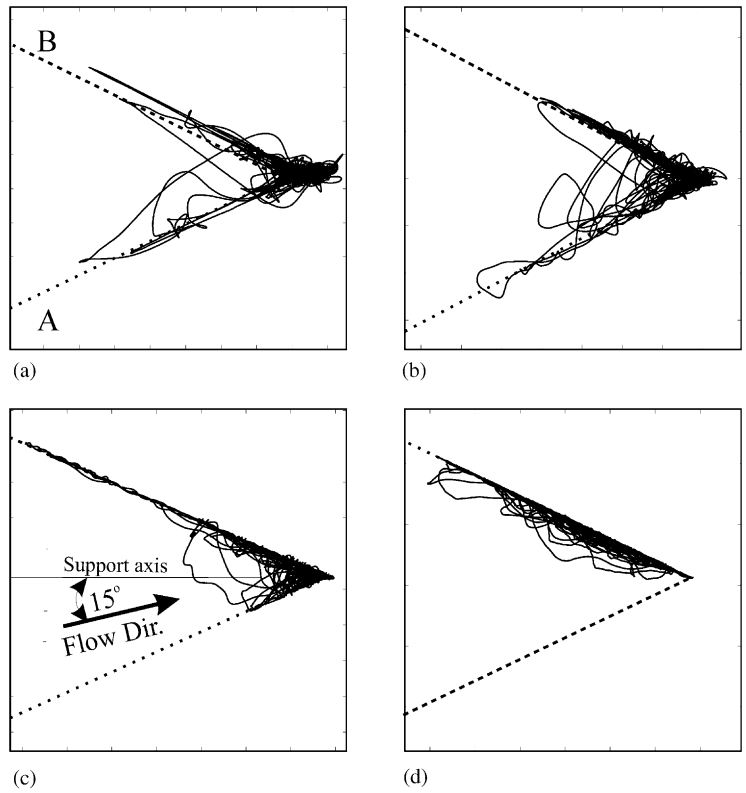
Fig. 13. Orbital tube motion for a 15° flow angle at various dimensionless clearance: (a) 0.15; (b) 0.25; (c) 0.35; and (d) 0.6.
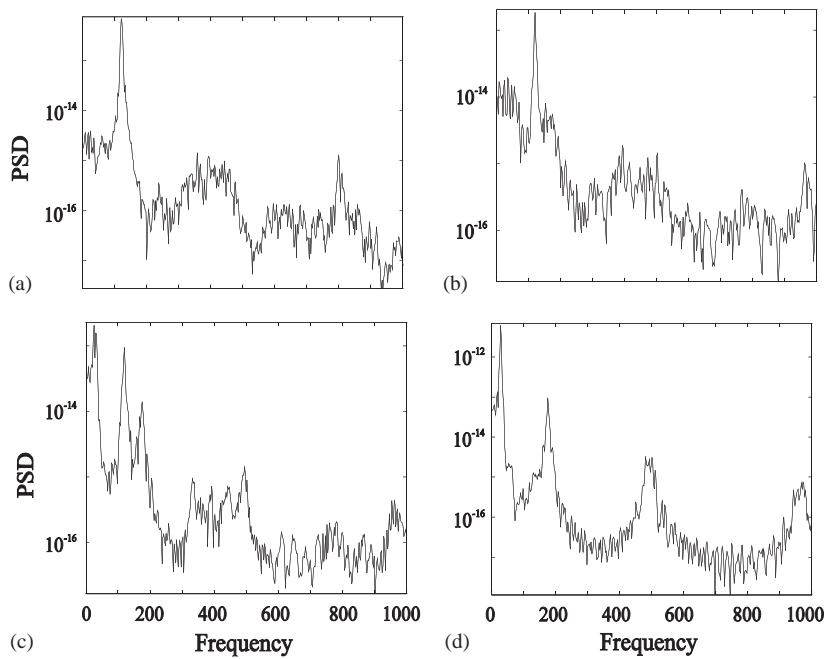
Fig. 14. Response spectra for various dimensionless clearances (30° flow angle): (a) 0.01; (b) 0.25; (c) 0.35; and (d) 1.1.

0.25, in addition to the 122 Hz peak, two narrow band peaks appear at 28 and 176 Hz. These correspond to the natural frequencies of the unconstrained configuration, Fig. 14(b). As the clearance increases further, the amplitude of the 28 Hz mode increases and becomes sharper while the amplitude of the 122 Hz mode decreases. At a clearance of approximately 0.3, the 28 Hz peak becomes dominant, Fig. 14(c). The first constrained mode (122 Hz) vanishes at a dimensionless clearance of 0.8. At this point, the response spectrum is essentially composed of the linear unconstrained modes (28, 176, and 492 Hz) as shown in Fig. 14(d). It should be noted that for the symmetric cases (0° and 90° flow angles), the tube dynamic response spectra are less complex than those observed for other flow angles, as can be seen by comparing Figs. 14 and 5.

3.6. Effect of the support offset

Hassan et al. (2002) presented the results of a simulation with 10% support offset. The results were sufficiently complex that a more thorough study was considered appropriate. Support offset (e) is defined as the axial distance between two successive pairs of flat bars as shown in Fig. 15. Support offset values are presented as percentages of the tube's length ranging from 0% to 30%. For each of these support offset values, sixteen radial clearance values are investigated. These simulations were carried out assuming a tube held by a loose RFB support with the crossflow assumed to be at a 0° angle with the support axis. Pair B was set at the tip of the tube, while pair A was given a different location along the span towards the fixed end to produce the desired offset. Note that for RFB supports with offset, the effective distance between one pair of supports and the tube's fixed end will be different for each pair. Additionally, since the support pairs are not orthogonal to each other (as in the case of SFB supports), orthogonal tube modes will be coupled through the supports. Thus, the tube dynamics will be very complex.

The contact between the tube and a specific support pair depends on the location of this pair along the span. The contact ratio for both pairs is therefore the same when the support offset is zero. As a support offset is introduced, the tube maintains an unequal contact ratio with both pairs. Fig. 16(a) depicts the contact ratio between the tube and support pair A for various support offset values. For a given dimensionless clearance in the range of 0 to 0.3, the contact ratio increases slightly as the support offset increases. This is attributed to the fact that a vibration node is created at the tip of the tube by support pair B, and hence the displacement in the plane of pair B is higher towards the mid-span. A higher offset is created by placing pair A away from the tip and closer to the mid-span. A higher tube response results in a higher contact ratio at pair A. As was mentioned earlier, if the clearance is increased, the tube loses its effectiveness and a mode switch occurs. This produces a different displacement distribution along the tube's span resulting in the maximum displacement being at the tip of the tube. For higher clearances values, increasing the support offset decreases the contact ratio between the tube and pair A. Moreover, the introduction of these offsets does not change the general behaviour of the contact ratio as a function of the clearance. Introducing an offset results in a region of continuous contact for a range of small clearances. For example, when the support offset is 6.7%, the tube remains in continuous contact with pair A up to a dimensionless clearance of approximately 0.2. As the offset increases, the tube maintains continuous contact over a larger clearance range.

Fig. 16(b) depicts the contact ratio between the tube and pair B, which is similar to that with pair A although it is slightly higher for larger clearances. This is because the effective support dominating the tube dynamics is located at the tip of the tube. As the clearance increases, the tube has less contact with support A, and more contact with support B. This can be illustrated by plotting the duty factor α versus the dimensionless clearance. The duty factor α is defined as follows:

$$\alpha = \frac{R_A}{R_B} \tag{8}$$

where R_A and R_B are the contact ratios at pair A and pair B, respectively. Fig. 17 depicts the duty factor for various support offsets. For a 0% offset, the contact ratio is the same for pair A and pair B. Therefore, the duty factor is unity for all clearance values. As offset is introduced, the duty factor is unity up to a certain dimensionless clearance, then it decreases sharply. The larger the offset is, the smaller the duty factor *á* will be for clearances above about 0.2. At some value of offset which increases with increasing clearance, contact is lost as the supports become inactive.

The dimensionless impact forces at support pairs A and B are shown in Figs. 18(a) and (b), respectively. Note that the impact force (vertical) scales are different in these figures. The general behaviour of the dimensionless impact force is maintained for all support offset values. The introduction of the support offset increases the r.m.s. impact force at pair A, Fig. 18(a), in the range of dimensionless clearances up to 0.2. On the other hand, the offset decreases the impact force slightly at pair B, Fig. 18(b). The effect of the support offset on the r.m.s. impact forces diminishes beyond a dimensionless clearance of about 0.4 at which the mode switch is occurring.
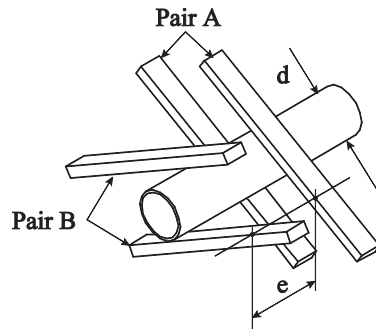
Fig. 15. Tube in a lattice-bar support with an offset.

(a)

(b)
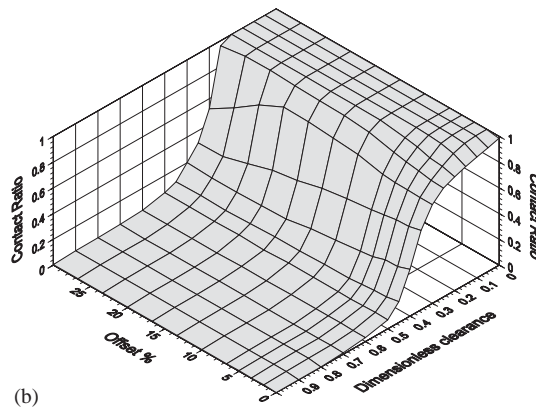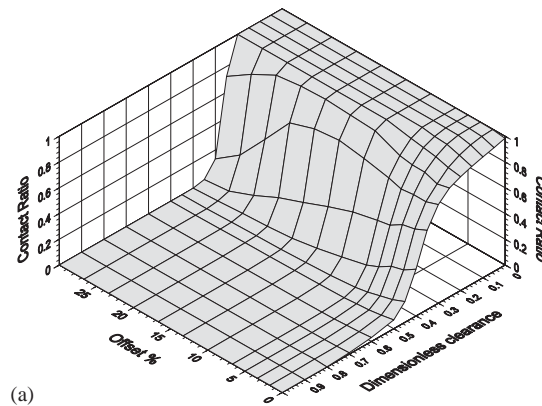
Fig. 16. Effect of the support offset on the contact ratio between the tube and the support: (a) pair A and (b) pair B.

The behaviour of a tube with a support offset is very complex. The tube response at a particular clearance and offset is composed of a combination of modes. These modes correspond to the possible linear subsystems, i.e., the unconstrained system, the fully constrained system, the system with support-active at pair A, or the system with support-active at pair B. The term support-active at pair B means that the tube is hinged at pair B and can respond in the plane containing the flat bars of pair A. Similarly, the term support-active at pair A means that the tube is hinged at pair A and the tube responds in the plane containing the flat bars of pair B. The natural frequencies of the tube with support-active at pair A are shown in Table 2 for various support offsets.

There are three main patterns of tube response observed in the range of support offsets under consideration. For each of these patterns, a sample of response spectra is presented. The tube response spectra for a support with a 5% offset are
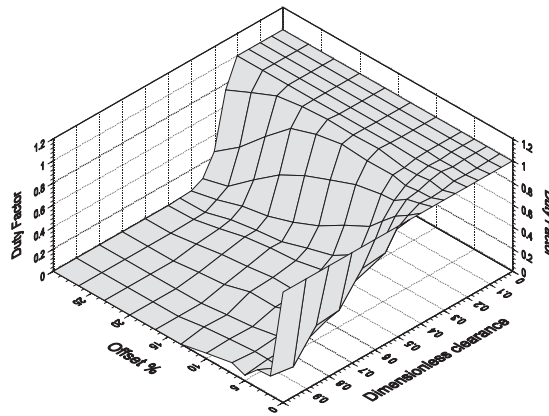
Fig. 17. Effect of the support offset on the pair contact duty factor.

(a)

(b)
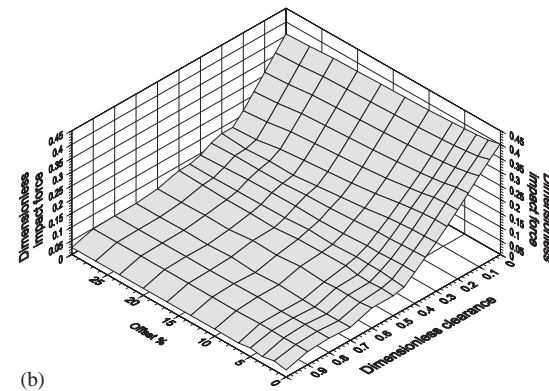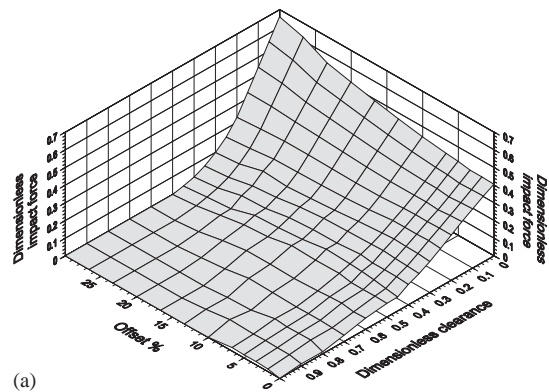
Fig. 18. Effect of the support offset on the r.m.s. impact force: (a) pair A and (b) pair B.

shown in Fig. 19. For a small dimensionless clearance of 0.001, Fig. 19(a) shows peaks at 123 and 137 Hz corresponding to the fundamental frequency of the support-active modes for pairs B and A, respectively. The amplitude of the 137 Hz peak is larger than that of the 123 Hz peak. As the dimensionless clearance is increased, the amplitude of the first peak at 123 Hz increases gradually, Fig. 19(b). At a larger dimensionless clearance (0.35), a narrow-band peak centred around a frequency of 127 Hz appears instead of distinct peaks at 123 Hz and 137 Hz, Fig. 19(c). At a larger dimensionless clearance (0.4), the band width of the fundamental peak increases, while its amplitude decreases, Fig. 19(d). At this point, the system is at the point of mode switch. With a further increase in clearance, two peaks appear at 47 Hz and 165 Hz, Fig. 19(e). Moreover, the response spreads over a wider range of frequencies around the

Table 2
Natural frequencies for different support offset values for support-active at pair A (support-active at pair B corresponds to 0% offset)

Offset (%)	Mode 1	Mode 2	Mode 3
0	122	398	831
1.67	127	413	861
3.33	132	426	888
5	137	442	919
6.7	140	454	941
10	150	480	962
13.3	160	492	881
16.7	169	470	776
20	175	418	756
23.33	175	372	784
26.67	167	350	833
30	152	349	891
Support-inactive	28	176	492

first unconstrained mode. For clearances above about 0.6, the dominant response is in the unconstrained fundamental mode at 28 Hz as seen in Fig. 19(f).

The tube response spectra in the case of a support with a 16.7% offset are shown in Fig. 20. The tube response spectra for a small dimensionless clearance (0.001) is shown in Fig. 20(a). This is a wide-band response which is spread over a range of frequencies (0–200 Hz). At a higher clearance (0.25), two well-separated peaks form at frequencies of 120 and 167 Hz. Each of these peaks corresponds approximately to the support-active mode of one of the pairs, Fig. 20(b). The amplitude of the first peak, occurring at 120 Hz, is larger than that of the second peak, which occurs at 167 Hz. As the clearance increases, the amplitude of the mode which corresponds to the support-active mode at pair A increases, Fig. 20(c). This behaviour continues up to a dimensionless clearance of 0.35. At this clearance, the system approaches the point of mode switch as shown in Fig. 20(d). At this point, the two peaks are not well separated, and the response is spread over a wider range of frequencies. For larger clearances, Fig. 20(e), the PSD of the tube response contains peaks at frequencies of 35, 175, and 495 Hz. These frequencies are approximately the first three natural frequencies of the fixed-free configuration. As the clearance increases further, these frequencies approach the exact values of the natural frequencies of the unconstrained system, although the first mode response dominates as seen in Fig. 20(f).

Fig. 21 shows the lift response spectra in the case of a tube with a 23.33% support offset. For a small dimensionless clearance, the lift response spectrum, Fig. 21(a), contains a peak around 251 Hz, which corresponds to the case in which both pairs A and B are active, i.e., the tube has pinned supports at both locations A and B. An increase in the dimensionless clearance causes the around 251 Hz peak to broaden and decrease gradually. Concurrently, another peak appears at a frequency around 110 Hz, Fig. 21(b). At a clearance of 0.3, the peak at 251 Hz vanishes and another peak appears around the frequency of the support-active mode for pair A, Fig. 21(c). With further increase in clearance, the fundamental unconstrained mode appears while peaks at around 100 Hz and 125 Hz dominate, Fig. 21(d). At a clearance of about 0.4, the mode switch take places as in Fig. 21(e) which shows the first three unconstrained modes. With clearances larger than about 0.5, the dominant frequency is that of the fundamental modes of the unconstrained system.

The predicted dimensionless normal work rates are presented in Fig. 22. The introduction of an offset has a dramatic effect on the normal work rate. For a given dimensionless support clearance in the range of 0–0.3, increasing the support offset causes the normal work rate at pair A to increase rapidly as shown in Fig. 22(a). This behaviour is maintained for a support offset in the range of 0–10% and is attributed to the amount of sliding motion permitted in the plane of pair A. When the offset is zero, the tube sliding motion on pair A meets two types of resistance: (a) the friction opposing the tube's motion in both directions, and (b) the flat bar belonging to pair B. As the offset increases, the second constraint becomes less effective since it restrains the tube at a point away from the plane containing pair A. Pair B creates a vibration node at the tip of the tube, and in the plane of pair A where the only resistance to the sliding motion is friction. This situation is applicable as long as the clearance is small enough to permit a support-active mode at the tube tip (pair B). The tube vibration is mainly in the first constrained mode with a frequency of approximately 123 Hz. Therefore, the sliding velocity, which is directly related to the frequency of oscillation, depends on the location of the effective support on the tube and a higher velocity component in this plane is therefore obtained for a larger offset. Moreover, the sliding velocity also depends on the degree of participation of this mode in the overall system response. For instance, the participation of this mode in the system's response, as indicated by the PSD of the tube
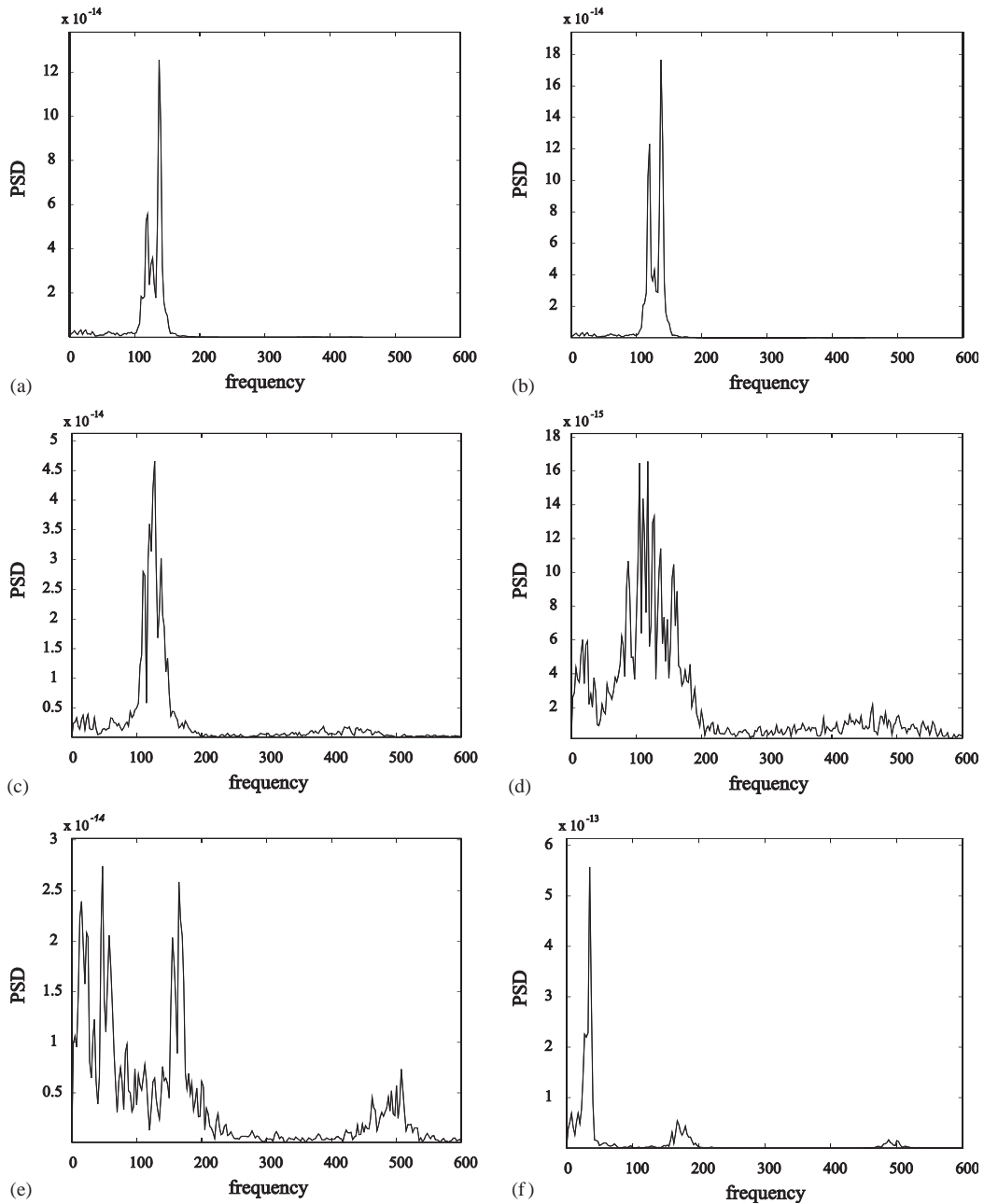
Fig. 19. Response spectra of a tube lattice-bar support (5% offset) at various dimensionless clearance values: (a) 0.001; (b) 0.15; (c) 0.35; (d) 0.4; (e) 0.45; and (f) 0.6.

displacement, increases as the offset increases. On the other hand, offsets larger than 10% result in a gradual decrease in the dimensionless work rate for pair A. This is attributed to the response of the tube, which has a broadband response covering a low range of frequencies. Now, as the clearance increases, the effectiveness at pair A is reduced. This translates to a slight decrease in the vibration frequency for a range of dimensionless clearances up to 0.3. In addition, the r.m.s. impact force decreases linearly as the dimensionless clearance increases. Therefore, the normal work rate, which is the average product of the impact force and the sliding velocity, decreases almost linearly for this range of dimensionless clearances. The frequency decreases dramatically approaching the dimensionless clearance at which the
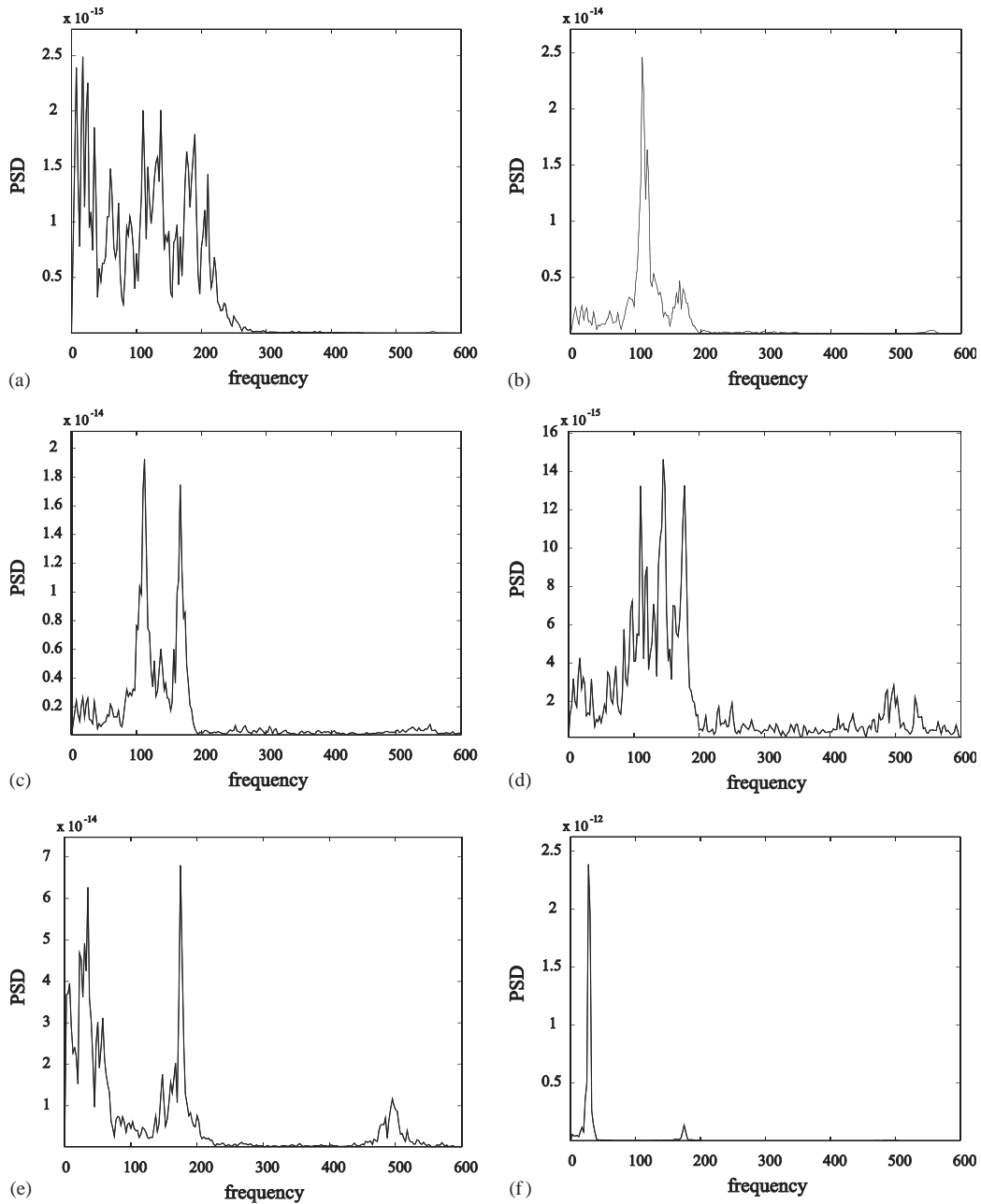
Fig. 20. Response spectra of a tube lattice bar support (16.67% offset) at various dimensionless clearance values: (a) 0.001; (b) 0.25; (c) 0.3; (d) 0.35; (e) 0.45; and (f) 0.7.

mode switch occurs. This reflects on the work rate, which decreases sharply as it approaches the mode switch. Moreover, the reduction in the r.m.s. impact force contributes to a reduction in the normal work rate.

Fig. 22(b) shows the normal work rate at pair B. Work rate is created through sliding the tube along the plane containing pair B. For small clearances, this sliding increases with offset as pair A creates a nodal point at its location. This results in an increase in the normal work rate produced at pair B which continues to an offset value of 6.67%, after which the normal work rate decreases. In addition, for offsets greater than about 20%, the work rate peaks sharply at a dimensionless clearance of approximately 0.35. At this combination of clearance and offset, pair A produces an effective node and shows a very small work rate while substantial sliding occurs at pair B and the work rate is very high.
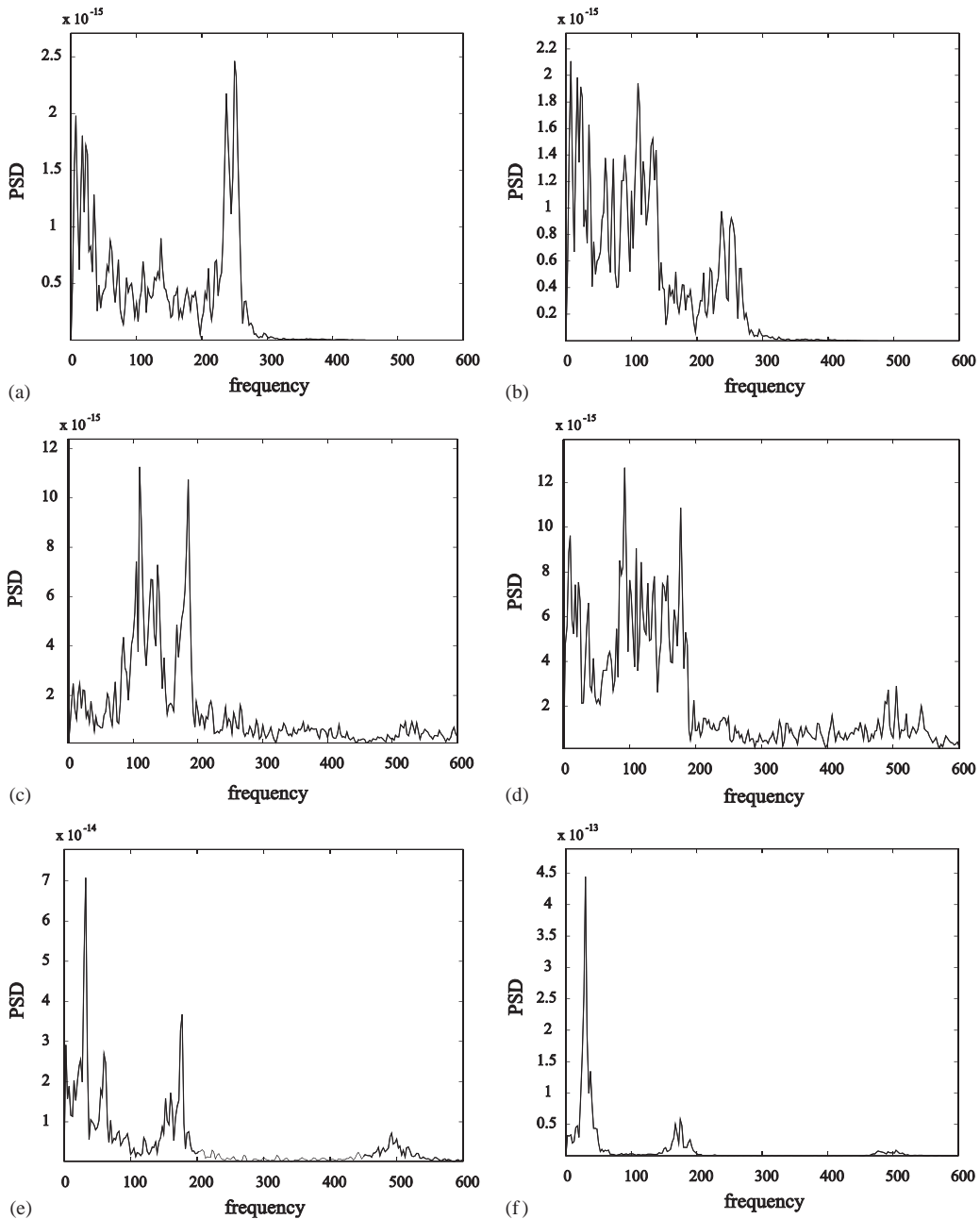
Fig. 21. Response spectra of a tube lattice-bar support (23.33% offset) at various dimensionless clearance values: (a) 0.001; (b) 0.15; (c) 0.3; (d) 0.35; (e) 0.4; and (f) 0.5.

4. Conclusions

In this paper, numerical simulations of a loosely supported tube excited by turbulence were conducted. The effects of the tube-to-support clearance, support geometry, flow orientation, and support offset on the tube response, were investigated. Under the conditions of small preload and no substantial initial eccentricity, a relatively simple friction model, VLFM, was shown to give an excellent prediction of tube response, impact force and contact ratio as well as a slightly conservative estimate of the work rate.
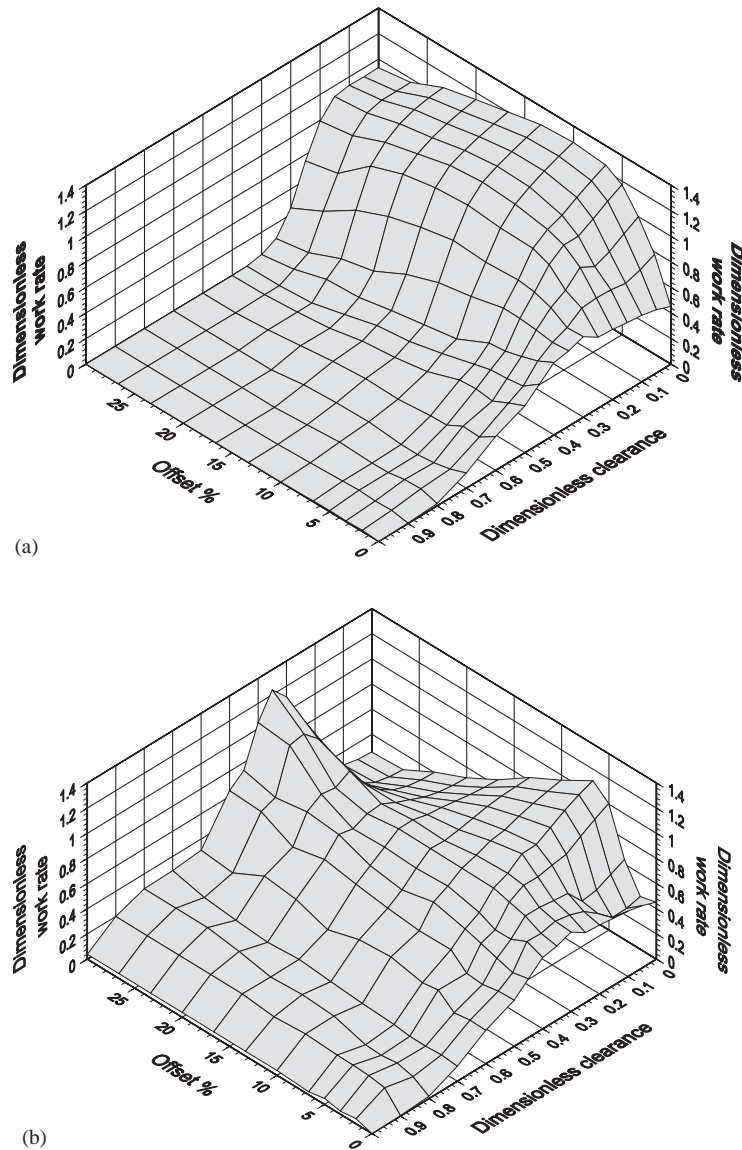
Fig. 22. Effect of support offset on the normal work rate: (a) pair A and (b) pair B.

The dynamics of turbulence excited, loosely supported tubes are very complex and strongly influenced by support clearance, geometry, flow orientation and support bar offset. However, it is possible to draw some general conclusions.

1. Regardless of the support geometry, increasing the support clearance increases the normal work rate as long as the support is active. Thus, minimizing tube-to-support clearance is beneficial in terms of reducing wear in heat exchangers.
2. Wear is generated by a combination of normal force and sliding along a tube's support. Thus, a worst case (higher work rate) occurs when the flow is normal to a support pair and the clearance is large enough to permit tube sliding along the support in the lift direction. For a given clearance, the wear rate will be at a minimum when the drag force of the flow tends to force a tube symmetrically into a corner of SFB or RFB supports.
3. Offset of RFB supports produces nonlinear coupling of tube modes and even greater complexity in tube dynamics. Increasing offset increases normal work rate since constraint of the tube by one support increases sliding contact with the adjacent support. Thus, wear should be minimized by minimizing support offset.

4. For small clearance, rhomboid flat supports with small offsets provide greater tube restraint and therefore less work rate than drilled hole or square flat bar supports.

References

Antunes, J., Axisa, F., Beaufils, B., Guilbaud, D., 1990. Coloumb friction modelling in numerical simulations of vibration and wear work rate of multispan tube bundles. Journal of Fluids & Structures 4, 287–304.

Axisa, F., Desseaux, A., Gibert, R., 1984. Experimental study of tube/support impact forces in multi-span PWR steam generator tubes. In: Proceedings of Symposium on Flow-Induced Vibrations, ASME Winter Annual Meeting, Vol. 3, New Orleans. ASME, New York, pp. 139–148.

Axisa, F., Antunes, J., Villard, B., 1988. Overview of numerical methods for predicting flow-induced vibration and wear of heat exchanger tubes. ASME Journal of Pressure Vessel Technology 110, 6–14.

Blevins, R., 1975. Vibration of a loosely held tube. Journal of Engineering for Industry 97, 1301–1304.

Cai, Y., Chen, S., 1993. Chaotic vibrations of nonlinearly supported tubes in crossflow. ASME Journal of Pressure Vessel Technology 115, 128–134.

Chen, S., 1978. Crossflow-induced vibrations of heat exchanger tube banks. Nuclear Engineering and Design 47, 67–86.

Chen, S., Jendrzjczyk, J., Wambsganss, M., 1985. Dynamics of tubes in fluid with tube-baffle interaction. ASME Journal of Pressure Vessel Technology 107, 7–17.

Connors, H., Kramer, F., 1991. U-bend shaker test investigation of tube-AVB wear potential. In: Institution of Mechanical Engineers, International Conference on Flow Induced Vibrations, IMechE 1991-6, Brighton, UK. IMECHE, London, pp. 57–67.

Dokainish, M., 1988. Incremental nonlinear dynamic analysis program: verification manual. McMaster University, Canada.

Fisher, N., Ingham, B., 1989. Measurement of tube-to-support dynamic forces in fretting-wear rigs. ASME Journal of Pressure Vessel Technology 111, 385–393.

Fisher, N., Olesen, M., Rogers, R., Ko, P., 1989. Simulation of tube-to-support dynamic interaction in heat exchange equipment. ASME Journal of Pressure Vessel Technology 111, 378–384.

Fisher, N., Pettigrew, M., Rogers, R., 1991. Fretting wear damage prediction in the inlet region of nuclear steam generators. In: Institution of Mechanical Engineers, International Conference on Flow Induced vibrations, IMechE 1991-6, Brighton, UK. IMECHE, London, pp. 149–158.

Fricker, A., 1992. Numerical analysis of the fluidelastic vibration of a steam generator tube with loose supports. Journal of Fluids and Structures 6, 85–107.

Haessig, D., Friedland, B., 1991. On the modeling and simulation of friction. Journal of Dynamic Systems, Measurements and Controls 113, 354–362.

Haslinger, K., Steininger, D., 1984. Steam generator tube/support plate interaction characteristics. In: Proceedings of Symposium on Flow-Induced Vibrations, ASME Winter Annual Meeting, Vol. 3, New Orleans. ASME, New York, pp. 9–14.

Haslinger, K., Steininger, D., 1995. Experimental characterization of sliding and impacting friction coefficients between steam generator tubes and AVB supports. Journal of Sound and Vibration 181, 851–871.

Haslinger, K., Martin, M., Steininger, D., 1987. Pressurized water reactor steam generator tube wear prediction utilizing experimental techniques. In: R. King (Ed.), Proceedings of BHRA Conference on Flow-Induced Vibrations, K2, Bowness-on-Windermere, UK. BHRA, Cranfield, pp. 437–448.

Hassan, M., Weaver, D., Dokainish, M., 2002. A simulation of the turbulence response of heat exchanger tubes in lattice-bar supports. Journal of Fluids and Structures 16, 1145–1176.

Hunt, K., Crossley, F., 1975. Coefficient of restitution interpreted as damping in vibroimpact. ASME Journal of Applied Mechanics 43, 440–445.

Karnopp, D., 1985. Computer simulation of stick-slip friction in mechanical dynamic systems. ASME Journal of Dynamic Systems, Measurements and Controls 107, 100–103.

Mureithi, N., Price, S., Païdoussis, M., 1994a. The post-Hopf-bifurcation response of a loosely supported cylinder in an array subjected to cross-flow Part I: experimental results. Journal of Fluids and Structures 8, 833–852.

Mureithi, N., Païdoussis, M., Price, S., 1994b. The post-Hopf-bifurcation response of a loosely supported cylinder in an array subjected to cross-flow. Part II: theoretical model and comparison with experiments. Journal of Fluid and Structures 8, 853–876.

Mureithi, N., Païdoussis, M., Price, S., 1995. Intermittency transition to chaos in the presence of a loosely supported cylinder in an array in cross-flow. Chaos, Solitons and Fractals 5, 847–867.

Oengören, A., Ziada, S., 1995. Vortex shedding, acoustic resonance and turbulent buffeting in normal triangle tube arrays. In: Bearman, P. (Ed.), Flow-Induced Vibrations. A. Balkema, Rotterdam, pp. 295–313.

Païdoussis, M., 1982. A review of flow-induced vibrations in reactors and reactor components. Nuclear Engineering and Design 74, 31–60.

Païdoussis, M., Li, G., 1992. Cross-flow-induced chaotic vibrations of heat-exchanger tubes impacting on loose supports. Journal of Sound and Vibration 152, 305–326.

Pettigrew, Gorman, 1978. Vibration of heat exchanger tube bundles in liquid and two-phase cross-flow. In: Chen, P.Y. (Ed.), Proceedings of Flow-Induced Vibrations Design Guidelines 1981, PVP-Vol. 52, Denver, CO, USA. ASME, New York, pp. 89–110.

Rao, M., Gupta, G., Eisinger, F., Hibbitt, H., Steininger, D., 1987. Computer modeling of vibration and wear multispan tubes with clearances at tube supports. In: R. King (Ed.), Proceedings of BHRA Conference on Flow-Induced Vibrations, K3, Bowness-on-Windermere, UK. BHRA, Cranfield, pp. 449–465.

Rogers, R., Pick, R., 1977. Factors associated with support plate forces due to heat exchanger tube vibratory contact. Nuclear Engineering and Design 44, 247–253.

Sauvé, R., Teper, W., 1987. Impact simulation of process equipment tubes and support plates-a numerical algorithm. ASME Journal of Pressure Vessel Technology 109, 70–79.

Tan, X., Rogers, R., 1996. Dynamic friction modelling in heat exchanger tube simulations. In: M. Pettigrew (Ed.), Flow-Induced Vibrations 1996, PVP-Vol. 328, Montréal. ASME, New York, pp. 347–358.

Weaver, D., Fitzpatrick, J., 1988. A review of cross-flow induced vibrations in heat exchanger tube arrays. Journal of Fluids and Structures 2, 73–93.

Weaver, D., Schneider, W., 1983. The effect of flat bar supports on the crossflow induced response of heat exchanger U-tubes. ASME Journal of Pressure Vessel Technology 105, 775–781.

Yetisir, M., Weaver, D., 1986. The dynamics of heat exchanger U-bend tubes with flat-bar supports. ASME Journal of Pressure Vessel Technology 108, 406–412.

Yetisir, M., Mckerrow, E., Pettigrew, M., 1997. Fretting wear damage of heat exchanger tubes: a proposed damage criterion based on tube vibration response. In: M. Païdoussis et al. (Eds.), Fourth International Symposium on Fluid–Structure Interactions, Aeroelasticity, Flow-Induced Vibration and Noise, Dallas, Vol. 2. ASME, New York, pp. 291–299.